

1

2

3 **DUSP6 inhibition overcomes Neuregulin/HER3-driven therapy
4 tolerance in HER2+ breast cancer**

5

6 Majid Momeny^{1,2§}, Mari Tienhaara^{3,4}, Mukund Sharma^{1,4}, Deepankar Chakroborty^{3,4},
7 Roosa Varjus¹, Iina Takala^{3,4}, Joni Merisaari¹, Artur Padzik¹, Andreas Vogt⁵, Ilkka
8 Paatero¹, Klaus Elenius^{3,4}, Teemu D. Laajala⁶, Kari J. Kurppa^{3,4}, Jukka
9 Westermarck^{1,4,§}

10

11 ¹Turku Bioscience Centre, University of Turku and Åbo Akademi University, Turku,
12 Finland

13 ²The Brown Foundation Institute of Molecular Medicine, McGovern Medical School,
14 The University of Texas Health Science Center at Houston, TX, USA.

15 ³Medicity Research Laboratories, Faculty of Medicine, University of Turku, Turku,
16 Finland

17 ⁴Institute of Biomedicine, University of Turku, Turku, Finland

18 ⁵University of Pittsburgh Drug Discovery Institute, Department of Computational and
19 Systems Biology, Pittsburgh Technology Center, Pittsburgh, PA, USA

20 ⁶Department of Mathematics and Statistics, University of Turku, Turku, Finland

21

22

23 [§]Co-corresponding authors: jukwes@utu.fi, majid.momeny@uth.tmc.edu

24

25

26

27 **Abstract**

28

29 Despite clinical benefits of tyrosine kinase inhibitors (TKIs) in cancer, most tumors
30 can reactivate proliferation under TKI therapy. Here we present transcriptional
31 profiling of HER2+ breast cancer cells transitioning from dormant drug tolerant cells
32 to re-proliferating cells under continuous HER2 inhibitor (HER2i) therapy. Focusing
33 on phosphatases, expression of dual-specificity phosphatase DUSP6 was found
34 inhibited in dormant cells, but strongly induced upon re-growth. DUSP6 expression
35 also selectively associated with poor patient survival in HER2+ breast cancers.
36 DUSP6 overexpression conferred apoptosis resistance, whereas its pharmacological
37 blockade prevented therapy tolerance development under HER2i therapy. DUSP6
38 targeting also synergized with clinically used HER2i combination therapies.
39 Mechanistically DUSP6 is a positive regulator of HER3 expression, and its impact
40 on HER2i tolerance was mediated by neuregulin-HER3 axis. *In vivo*, genetic
41 targeting of *DUSP6* reduced tumor growth in brain metastasis model, whereas its
42 pharmacological targeting induced synthetic lethal therapeutic effect in combination
43 with HER2i. Collectively this work demonstrates that *DUSP6* drives escape from
44 HER2i-induced dormancy, and that DUSP6 is a druggable target to overcome
45 HER3-driven TKI resistance.

46 **Keywords:** Non-genetic drug tolerance, Lapatinib, Neratinib, BCI, FOXM1

47

48

49 **The paper explained:**

50

51 **Problem**

52 The molecular mechanisms for the acquisition of resistance to HER2-targeted
53 therapies in breast cancer are still elusive, especially when the drug-tolerant
54 persister cells start to regrow under the treatment.

55 **Results**

56 The oncogenic phosphatase DUSP6 is increased in the drug-tolerant emerging
57 persister cells and plays central roles in the acquisition of HER2i resistance.
58 Moreover, DUSP6 blockade potentiates therapeutic sensitivity in the primary
59 resistant models via inhibition of the HER3 signaling pathway. Inhibition of DUSP6
60 offers advantages over AKT blockade, including induction of apoptotic cell death,
61 preempting ligand-induced rescue, and inhibition of HER3. Ultimately, DUSP6
62 inhibition reverses HER2i resistance *in vivo* and reduces the outgrowth of HER2+
63 cell in the brain metastasis models.

64 **Impact**

65 These findings have implications in the clinical management of HER2+ breast cancer
66 and warrant development and clinical investigation of DUSP6 inhibitors in
67 combination with HER2-directed therapies in the patients.

68

69

70

71 **Introduction**

72

73 To develop therapeutic resistance, tumor cells undergo distinct evolutionary stages,
74 starting with induction of dormancy and non-genetic drug tolerance, followed by
75 epigenetic changes and finally resistance-conferring genetic mutations (De Conti *et*
76 *al*, 2021; Hata *et al*, 2016; Marine *et al*, 2020). These different phases were originally
77 demonstrated for EGFR-targeted therapies in non-small cell lung cancer (NSCLC)
78 cells (Sharma *et al*, 2010), but the concept has been expanded more recently to
79 other malignancies including HER2+ breast cancer (Chang *et al*, 2022; De Conti *et*
80 *al.*, 2021; Dhimolea *et al*, 2021; Hata *et al.*, 2016; Kurppa *et al*, 2020; Sharma *et al.*,
81 2010). Based on these studies, there is ample of omics data from dormant cells (also
82 called as drug tolerant persisters; DTPs) from different cancer types treated with
83 variety of therapies. However, our understanding of the molecular mechanisms
84 behind the regrowth of DTPs under continuous therapy is still rudimentary.
85 Especially, to our knowledge there are no published studies describing
86 transcriptional landscapes of transition from DTP to drug tolerant expanding cells
87 (DTEP), or transition of DTEP cells to long term resistant (LR) cells upon TKI
88 therapies.

89

90 The human epidermal growth factor receptor 2 (HER2; encoded by *ERBB2*) is
91 overexpressed in ~15-25% of human breast cancers and associates with a poor
92 patient survival (Arteaga & Engelman, 2014; Haikala & Janne, 2021). HER2 belongs
93 to the ERBB family of receptor tyrosine kinase (RTK) with four members: HER1
94 (EGFR), HER2, HER3 and HER4. Upon ligand binding, the ERBB receptors homo-
95 and heterodimerize and activate downstream signaling pathways including PI3K/AKT

96 and RAS/MAPK/ERK, which regulate cell proliferation, survival and the metastatic
97 dissemination (Arteaga & Engelman, 2014; Haikala & Janne, 2021). Multiple HER2-
98 targeted therapies, including the monoclonal antibody trastuzumab and small
99 molecule tyrosine kinase inhibitors (TKIs) have been approved for the treatment of
100 HER2-overexpressing (HER2+) breast cancer (Goutsouliak *et al*, 2020). Application
101 of anti-HER2 agents in combination with chemotherapy has significantly improved
102 the patients' outcome. However, patients initially responsive to the HER2 inhibitors
103 (HER2is) almost inevitably succumb to disease relapse (Goutsouliak *et al.*, 2020).
104 Moreover, HER2+ breast tumors have an inherent tendency to develop brain
105 metastasis, a significant clinical challenge for the treatment of these patients (Fecchi
106 *et al*, 2019). Therefore, there is a pressing need for novel and more efficacious
107 therapeutic strategies to overcome resistance to HER2is.

108

109 HER3 is an obligate heterodimerization partner for HER2 and plays essential roles in
110 HER2-driven tumorigenesis, and resistance to HER2is (Haikala & Janne, 2021;
111 Wilson *et al*, 2012). Consistent with the effects of HER3 overexpression, the HER3
112 ligand neuregulin (NRG, a.k.a Hereregulin; HRG) promotes trastuzumab resistance in
113 HER2+ breast cancer cells (Haikala & Janne, 2021). Importantly, the NRG-HER3
114 axis also promotes resistance to a wide range of TKIs and chemotherapies (Erjala *et*
115 *al*, 2006; Haikala & Janne, 2021; Knuefermann *et al*, 2003; Recondo *et al*, 2020;
116 Wilson *et al.*, 2012; Yonesaka *et al*, 2011). Despite the importance of HER3 in
117 cancer progression and therapy resistance, development of HER3 small molecule
118 inhibitors has been challenging due to its impaired kinase activity (Haikala & Janne,
119 2021; Xie *et al*, 2014). Moreover, the clinical activity of HER3 monoclonal antibodies
120 either as monotherapies or in combination with chemo- and targeted therapies have

121 been marginal (Cleary *et al*, 2017; Haikala & Janne, 2021; Schneeweiss *et al*, 2018).
122 To this end, there is a pressing need to identify novel strategies to inhibit HER3
123 activity and/or expression for the treatment of HER3-dependent human malignancies
124 (Gaborit *et al*, 2015; Haikala & Janne, 2021; Xie *et al.*, 2014).

125

126 There is emerging evidence that phosphatases are novel and “druggable” targets in
127 oncology (Lazo *et al*, 2018; Vainonen *et al*, 2021). Inhibition of oncogenic
128 phosphatases, or re-activation of tumor suppressor phosphatases, by small molecule
129 therapies halt tumor growth, retard malignant progression, and enhance therapeutic
130 sensitivity in various neoplasms (Lazo *et al.*, 2018; Vainonen *et al.*, 2021). Despite
131 this, the contribution of phosphatases to resistance to HER2is is still poorly
132 understood. Dual-specificity phosphatases (DUSPs) belong to the superfamily of
133 protein tyrosine phosphatases and dephosphorylate both tyrosines and serines or
134 threonines. A subgroup of the DUSPs are mitogen-activated protein kinase (MAPK)
135 phosphatases that selectively interact with and dephosphorylate the MAPKs
136 (Patterson *et al*, 2009; Zandi *et al*, 2022). For instance, DUSP6 displays a high
137 degree of substrate selectivity for the extracellular signal-regulated kinase (ERK), but
138 not P38 or c-Jun N-terminal kinase (JNK) (Zandi *et al.*, 2022). However, recent
139 studies indicate that at least some cancer relevant DUSP6 functions may be ERK-
140 independent (Kong *et al*, 2023). DUSP6 is indicated in clinical cancer progression,
141 and its genetic inhibition prevents tumor cell growth (Shojaee *et al*, 2015; Wu *et al*,
142 2018). Notably, DUSP6 is a druggable phosphatase (Korotchenko *et al*, 2014;
143 Molina *et al*, 2009; Vainonen *et al.*, 2021; Zandi *et al.*, 2022). The best characterized
144 DUSP6 inhibitor molecule BCI ((E)-2-Benzylidene-3-(cyclohexylamino)-2,3-dihydro-
145 1H-inden-1-one), is a semi-allosteric inhibitor of both DUSP1 and 6 that phenocopies

146 genetic DUSP6 inhibition in several cancer models (Kong *et al.*, 2023; Korotchenko
147 *et al.*, 2014; Molina *et al.*, 2009; Vainonen *et al.*, 2021). However, the role and
148 potential of therapeutic targeting of DUSP6 in overcoming resistance to HER2is is
149 currently unknown.

150

151 Here we present transcriptional analysis of HER2i treated HER2+ cancer cells upon
152 9 months of continuous HER2i treatment. In addition to revealing first global gene
153 expression programs associated with the DTP-DTEP and DTEP-LR therapy
154 tolerance transitions, we use complementary genetic and pharmacological
155 approaches to demonstrate that *DUSP6* has critical role in regrowth of DTEP cells
156 under HER2i therapies. Mechanistically, DUSP6 drives non-genetic HER2i tolerance
157 via regulation of HER3 expression, and by abrogating neuregulin-elicited apoptosis
158 resistance. Collectively our findings provide a strong pre-clinical rationale to further
159 advance in DUSP6 blockade for HER3 targeting in general, and especially for the
160 clinical management of HER2+ breast cancer patients with resistance to HER2i.

161

162

163 **Results**

164

165 **Development of acquired HER2i resistance by long-term treatment of drug**
166 **sensitive HER2+ breast cancer cells with lapatinib**

167

168 To model the full range of development of HER2i resistance starting from primary
169 sensitive phase, via drug-tolerant persister (DTP) development, and re-emergence of
170 proliferative drug-tolerant expanded persister (DTEP) cells, to long-term resistant
171 cells (LR), the HER2i sensitive cell line BT474, and its brain seeking variant BT474Br
172 (Zhang *et al.*, 2013), were exposed to therapeutically relevant 1 μM of lapatinib every
173 3 days for up to 9 months (Fig. 1A). Both cell lines followed a similar pattern of
174 lapatinib tolerance development, where at the 9-day timepoint only a few DTP cells
175 could be microscopically observed, whereas the emergence DTEP population took
176 about 6 months (Fig. 1A). Following this, the plates were fully populated by the LR
177 cells after 9 months of continuous lapatinib treatment (Fig. 1A). Importantly, in
178 addition to lapatinib, the LR clones of both BT474 and BT474Br displayed strong
179 cross resistance to tucatinib (a HER2i), afatinib (a HER2/EGFR inhibitor), and
180 neratinib (a HER2/HER4/EGFR inhibitor) (Figure EV1). This indicates that the
181 acquired resistance is not specific to lapatinib but is driven by a mechanism that is
182 generally relevant to the ERBB family of RTKs.

183

184 **Transcriptomic landscape of acquired lapatinib resistance in BT474 cells**

185

186 Recent studies have focused on the molecular characterization of DTP cells in
187 response to kinase inhibitor therapies (Chang *et al.*, 2022; Kurppa *et al.*, 2020;

188 Marsolier *et al*, 2022) but there is no published information about transcriptional
189 profiles of TKI treated cells at the DTP-DTEP or DTEP-LR transitions. To this end,
190 the transcriptional profiles from each functional state of lapatinib drug tolerance and
191 resistance development in BT474 cells were surveyed by bulk RNA-sequencing.
192 From three technical replicates per condition, and by using statistical criteria of
193 $|logFC|>2$ and Benjamini-Hochberg adjusted $p <0.05$, upregulation of 144, 1169 and
194 16 genes was found upon the control-DTP, DTP-DTEP, and DTEP-LR transitions of
195 BT474 cells, respectively (Fig. 1B, Dataset EV1). On the other hand, the number of
196 downregulated genes were 517, 930 and 28, respectively (Fig. 1B, Dataset EV1).
197 The highest number of differentially regulated genes upon the DTP-DTEP transition
198 indicates that this is the transition phase where the BT474 cell fate is most robustly
199 impacted during the resistance development. When assessing the patterns of gene
200 expression changes by unsupervised soft clustering analysis (Futschik & Carlisle,
201 2005), we identified six approximately similar size gene clusters with distinct
202 regulation patterns (Appendix Figure S1A). The genes included in these clusters are
203 listed in the Dataset EV2. Such regulation patterns indicate that neither gene
204 activation nor gene repression characterize lapatinib resistance development in
205 BT474 cells, but unique gene expression programs are involved in each of these
206 steps.

207

208 **Gene regulatory mechanisms and hallmarks associated with HER2i resistance
209 transitions**

210

211 To understand gene regulatory mechanisms controlling transitions between the
212 different phases on lapatinib tolerance and resistance development, we predicted the

213 transcription factor binding sites enriched on promoter regions of the differentially
214 regulated genes (Fig. 1B, Dataset EV3). Using FDR < 0.05 as a cut-off, the most
215 highly enriched transcription factor elements in genes downregulated upon the
216 control-DTP transition were E2F4, FOXM1, FLI1, E2F1 and NFYA (Fig. 1B, Dataset
217 EV3). Strikingly, most of these transcription factor binding sites were enriched also in
218 the genes significantly upregulated in DTEP cells (Fig. 1B in bold, Dataset EV3).
219 This indicates that these transcription factors are inactivated co-ordinately upon the
220 development of the DTP state and re-activated upon re-growth of the DTEPs. E2F4,
221 FOXM1 and E2F1 are all indicated in development and progression of breast cancer.
222 We validated inhibition of selected BT474 cell DTP FOXM1 and E2F target genes
223 across different HER2+ cells treated with lapatinib to reach the DTP state (Figure
224 EV2). On the other hand, binding sites for transcription factors CBX2, ESR1, TCF12
225 and ZNF217 were found significantly enriched in the genes downregulated upon
226 DTP to DTEP transition, whereas STAT1 and STAT2 were enriched among the
227 genes upregulated in LR cells as compared to DTEPs (Fig. 1B, Dataset EV3).

228

229 To identify cancer hallmark processes involved in each transition phase, the entire
230 transcriptomics data was re-analysed by Gene Set Variation Analysis (GSVA).
231 Consistent with recent evidence from other DTP models (Chang *et al.*, 2022;
232 Dhimolea *et al.*, 2021; Kurppa *et al.*, 2020), MYC signaling was inhibited in the
233 lapatinib-treated BT474 DTPs, but reactivated in DTEPs (Fig. 1C, gene sets 3 and
234 6). Similar gene regulation pattern was observed for E2F1 targets, G2/M checkpoint,
235 mTOR signaling, and androgen response (Fig. 1C, gene set 3), ROS signaling,
236 oxidative phosphorylation, and DNA repair (Fig. 1C, gene set 6). Interestingly, the
237 DTP-DTEP transition was associated also with downregulation of several cancer

238 hallmark gene sets, most apparently seen in set 4 where KRAS signaling, EMT,
239 WNT/β-catenin, and inflammatory response genes were all suppressed upon
240 proliferation reactivation (Fig. 1C). Additional hallmark gene sets regulated between
241 the lapatinib resistance development transitions are displayed in appendix figure
242 S1B.

243

244 Collectively these results demonstrate that unique gene clusters and biological
245 processes are involved in each step of lapatinib resistance development. This bulk
246 RNA-sequencing data provides a rich resource for future studies of gene regulatory
247 mechanisms in HER2i tolerance and resistance development. However, it is clear
248 that future single cell RNA sequencing studies are needed to understand clonality of
249 gene expression changes induced during these transitions.

250

251

252 **Phosphatase gene expression landscape in DTPs and DTEPs**

253

254 Recent data indicates that development of cancer therapy resistance is initiated by
255 non-genetic signaling rewiring mediated by post-translational regulation of
256 intracellular signaling pathways (De Conti *et al.*, 2021; Hata *et al.*, 2016; Marine *et*
257 *al.*, 2020). Protein phosphorylation is the most prevalent post-translational
258 modification in cancer cells, and cancer cell phosphoproteomes are regulated by
259 kinases and phosphatases. Whereas the role of kinases in non-genetic therapy
260 tolerance development has been extensively studied (Marine *et al.*, 2020), the
261 importance of phosphatases to development of non-genetic kinase inhibitor therapy
262 tolerance have been thus far poorly characterized. Therefore, we focused on the
263 dynamics of phosphatase gene regulation during lapatinib tolerance development.

264 Importantly, there were only four phosphatase genes (*CDC25A*, *CDC25C*, *DUSP6*
265 and *SYNJ1*) that were synchronously downregulated in DTP cells but upregulated in
266 DTEPs versus DTPs (Fig. 2A-C, Dataset EV1). We rationalized that these four
267 phosphatases might be particularly relevant for allowing the regrowth of the DTEP
268 population under continuous lapatinib treatment. Even though a large group of other
269 genes were found differentially regulated between the DTEP and LR populations
270 (Fig. 1B, Dataset EV1 and EV2), none of the phosphatase genes were significantly
271 regulated in the DTEP-LR transition (Dataset EV1). This indicates that regulation of
272 phosphatase gene expression could be primarily relevant to the early non-genetic
273 phases of acquired lapatinib resistance.

274
275
276 **Clinical association of *DUSP6* with poor prognosis HER2+ breast cancer**

277
278 Based on the above analysis, *CDC25A*, *CDC25C*, *DUSP6* and *SYNJ1* were the only
279 phosphatases that were significantly regulated during both therapy tolerance
280 transitions (Fig. 2A-C). To evaluate potential clinical relevance of the selected four
281 phosphatases in human breast cancer, we first examined their expression levels
282 across breast cancer subtypes in the METABRIC dataset (Dataref:(Pereira *et al*,
283 2016). Interestingly, *DUSP6* was the only one of these four phosphatases that was
284 selectively overexpressed in the target HER2+ subtype of breast cancers (Fig. 2D).
285 The closest functional orthologue for *DUSP6*, *DUSP1* did not show HER2+ selective
286 overexpression (Appendix Figure S2A). *DUSP6* overexpression in HER2+ breast
287 cancer was confirmed in the TCGA breast invasive carcinoma dataset (Dataref:
288 (Cerami *et al*, 2012; de Bruijn *et al*, 2023; Gao *et al*, 2013)(Appendix Figure S2B).
289 Further, when the 1082 breast invasive carcinoma samples from the TCGA BRCA-

dataset (Dataref: (Cerami *et al.*, 2012; de Bruijn *et al.*, 2023; Gao *et al.*, 2013) were divided to DUSP6high and DUSP6low groups based on their *DUSP6* mRNA expression levels, HER2+ and luminal A subtypes were clearly enriched among the DUSP6high samples (Fig. 2E). HER2 positivity was also found enriched among DUSP6high tumors based on HER2 immunohistochemistry of samples available for staining in the Breast Invasive Carcinoma (TCGA, Firehose legacy) dataset (Dataref: (Cerami *et al.*, 2012; de Bruijn *et al.*, 2023; Gao *et al.*, 2013) (Appendix Figure S2C).

297

To study the prognostic value of *DUSP6* expression in HER2+ breast cancers from the TCGA BRCA-dataset, the patients with high *ERBB2* (gene coding for HER2) expression were further divided into *DUSP6*high and low groups. Comparison of the survival outcomes between the two groups indicate that high *DUSP6* expression predicts poor overall and disease-free survival among HER2+ patients (Fig. 2F,G). In multivariable analysis of high *ERBB2* expressing tumors, increase in *DUSP6* expression and large tumor size (T4) remained significant independent prognostic factors (Appendix Figure S2D). However, *DUSP6* mRNA expression was neither a prognostic factor in Luminal B or Basal subtypes, nor across unselected breast cancer patient population (Appendix Figure S2E), further highlighting the selective connection between DUSP6 and HER2 in breast cancer progression.

309

Interestingly, luminal B cancers were clearly enriched in *DUSP6*low samples as compared to *DUSP6*high (Fig. 2E). Luminal B are estrogen receptor (ER) positive cancers that often also express HER2. Clinically luminal B cancers are less aggressive than HER2+ cancers. This data may suggest that DUSP6 has a role in suppressing ER positivity, and thereby increasing the relative numbers of HER2+

315 cancers over luminal B cancers. Although the details of this regulation remain
316 unclear, this hypothesis is supported by strongly decreased expression of ER protein
317 and *ESR1* mRNA, coding for ER, in HER2+ *DUSP6high* samples as compared to
318 HER2+ *DUSP6low* samples (Appendix Figure S2F,G).

319

320 These data demonstrate that DUSP6 is clinically associated with the aggressive
321 HER2+ breast cancer but may also have a broader role in defining breast cancer
322 subtype development.

323

324 **DUSP6 promotes the HER2i tolerance and DTP-DTEP transition under
325 continuous lapatinib treatment**

326

327 Clinical relevance of DUSP6 in HER2+ breast cancers among the four candidate
328 phosphatases differentially regulated at DTP-DTEP transition, together with the
329 feasibility of DUSP6 targeting by small molecules (Kong *et al.*, 2023; Korotchenko *et*
330 *al.*, 2014; Molina *et al.*, 2009; Vainonen *et al.*, 2021; Zandi *et al.*, 2022), motivated us
331 to select DUSP6 as the phosphatase to be focused in this study. We confirmed
332 differential expression of DUSP6 across different resistance acquisition transitions in
333 BT474 cells. Consistent with the RNA sequencing results (Fig. 2C), DUSP6 protein
334 expression was strongly induced upon the DTP-DTEP transition (Fig. 3A). While the
335 *DUSP6* mRNA levels were diminished in the fully resistant LR clones compared to
336 DTEPs (Fig. 2C), its protein levels remained robustly elevated presumably via post-
337 translational stabilization mechanisms (Fig. 3A). Validating that these effects were
338 not cell line specific, DUSP6 protein was also increased in BT474BrLR cells as
339 compared to the parental cells (Appendix Figure 3A). We further validated inhibition

340 of *DUSP6* upon DTP phase across independent set of lapatinib treated HER2+ cells
341 including BT474Br, and two cell lines (EFM192A, HCC1419) from (Data ref:(Chang
342 *et al.*, 2022)(GSE155342), or NSCLC, melanoma, and colorectal cancer cells *de*
343 *novo* treated with various TKIs (Fig. 3B). Therefore, inhibition of *DUSP6* expression
344 appears as a general mechanism associated with establishment of TKI-induced
345 therapy tolerance. Selected E2F1 and FOXM1 target genes were also confirmed to
346 be downregulated in TKI-treated NSCLC, MM, and CRC DTP cells (Appendix Figure
347 S3B). Notably, among the transcription factors differentially implicated upon HER2i
348 tolerance development (Fig. 1B), forkhead box transcription factor M1 (FOXM1) and
349 NFYA bind to *DUSP6* promoter (Dataset EV4), and coinciding with *DUSP6*
350 expression, *FOXM1* gene expression is downregulated in DTPs and upregulated in
351 DTEPs (Appendix Figure S3C). Functionally, a small molecule inhibitor of FOXM1
352 (FDI-6) (Wang *et al*, 2021) inhibited *DUSP6* expression in a time-dependent fashion
353 in BT474 cells (Appendix Figure S3D,E). Together with its role as breast cancer
354 oncogene involved in therapy resistance (Zhang *et al*, 2021), these data imply
355 FOXM1 as a viable candidate inducing *DUSP6* expression during the DTP-DTEP
356 transition.

357

358 To evaluate whether the hallmark gene sets co-regulated with *DUSP6* during therapy
359 tolerance transitions (Fig. 1C) could be functionally downstream of *DUSP6*, we
360 performed a RNAseq analysis from *DUSP6* depleted MDA-MB-453 cells and
361 compared these two gene sets. Notably, there was a marked overlap between
362 hallmark gene sets from these two conditions in which *DUSP6* expression was
363 suppressed (Fig. 1C versus Fig. 3C; overlapping gene sets highlighted in red).
364 Especially interesting finding was that the *DUSP6* knockdown cells displayed a gene

365 expression pattern linked to dormant cancer cells such as inhibition of MYC, E2F1
366 targets, and the PI3K/AKT/mTOR signaling, as well as activation of the interferon
367 response (Chang *et al.*, 2022; Dhimolea *et al.*, 2021; Kurppa *et al.*, 2020; Marine *et*
368 *al.*, 2020). The finding that siRNA-mediated *DUSP6* depletion (Fig. 3C) recapitulates
369 the gene expression profile in the lapatinib-induced DTP cells (Fig. 1C), clearly
370 indicates that inhibition of *DUSP6*-driven gene expression programs functionally
371 contribute to the HER2i-elicited growth inhibition.

372
373
374 To functionally validate that increased *DUSP6* expression in DTEP cells contributes
375 to their survival, we ectopically overexpressed *DUSP6* in BT474 cells, and subjected
376 the cells to treatment with lapatinib, neratinib, afatinib, or tucatinib. Importantly,
377 *DUSP6* overexpression was able to dampen both cell viability inhibition, and
378 apoptosis induction, by all four tested HER2is (Fig. 3D,E and Figure EV3A-D).
379 Mechanistically, the anti-apoptotic activity of *DUSP6* in lapatinib treated BT474 cells
380 appeared to be independent of ERK MAPK regulation, as overexpression of the KIM
381 mutant of *DUSP6* (R64A,R65A), incapable in ERK binding (Nichols *et al*, 2000), had
382 equally strong impact as the wild-type *DUSP6* (Fig. 3F and Appendix Figure S3F).
383 ERK-independent antiapoptotic activity for *DUSP6* in cancer cells was suggested
384 also recently (Kong *et al.*, 2023). As a complementary pharmacological approach,
385 BT474 cells were treated with lapatinib or neratinib alone, or in combination with
386 small molecule *DUSP6* inhibitor BCI for 6 months. BCI is a semi-allosteric inhibitor of
387 both *DUSP1* and *DUSP6* and several studies have demonstrated that BCI
388 phenocopies genetic *DUSP6* inhibition in cancer (Kong *et al.*, 2023; Ramkissoon *et*
389 *al*, 2019; Shojaee *et al.*, 2015). Notably, as compared to the monotherapies,
390 combination with BCI preempted the DTEP development in both lapatinib and

391 neratinib treated cells (Fig. 3G). Strongly indicative of selective drug interaction
392 rather than overall toxicity by BCI, the BCI used at the given concentration for 6
393 months did not kill all BT474 cells but potently synergized with the HER2is (Fig. 3G).
394 The fact that DUSP6 overexpression inhibited HER2i-elicited cell killing (Fig. 3E),
395 whereas BCI abrogated development of HER2i tolerant cells (Fig. 3G), strongly
396 support selective effects for BCI on DUSP6. Indeed, the role of DUSP1 as a primary
397 BCI target was overruled by the results that DUSP1 was neither expressed at the
398 protein level in BT474 cells (Fig. 3A), nor its mRNA was found differentially regulated
399 between any of the acquired resistance phases (Fig. 2A, B, Dataset EV1). In
400 harmony, DUSP1 overexpression had clearly weaker activity than DUSP6
401 overexpression in the rescue experiments (Figure EV3D). To further validate the
402 selectivity of BCI as a DUSP6 inhibitor, we generated *DUSP6* knockout (*DUSP6KO*)
403 MDA-MB-453 cells by CRISPR/CAS9 (Appendix Figure S3G). Indeed, three
404 independent single cell clones of *DUSP6KO* cells were significantly less sensitive to
405 BCI-elicited inhibition of cell viability as compared to the control cells (Appendix
406 Figure S3H).

407
408 Collectively, these results identify *DUSP6* downregulation to be functionally relevant
409 for establishment of the DTP phase, whereas its transcriptional induction contributes
410 to DTP-DTEP transition in lapatinib treated HER2+ cells.

411
412 **DUSP6 targeting kills HER2i resistant breast cancer cells and synergizes with**
413 **HER2i combination therapies**

415 After discovering the role for DUSP6 in the development of HER2i tolerance, we
416 wanted to address its role in HER2+ breast cancer cells with stable HER2i
417 resistance. To this end, we compared pharmacological DUSP6 targeting against a
418 library of available small molecule modulators of other phosphatases (Lazo *et al.*,
419 2018; Vainonen *et al.*, 2021). Across either HER2i resistant cells lines, inhibition of
420 cell viability by phosphatase targeting was observed only with DUSP6 inhibitor BCI,
421 its derivative BCI-215, and with FTY-720 that reactivates protein phosphatase 2A
422 (PP2A) by SET inhibition (Saddoughi *et al*, 2013)(Figure EV4). The phenocopying
423 results between BCI and BCI-215 is an important additional evidence for the
424 selectivity of BCI type of drugs towards DUSPs, as BCI-215 was demonstrated to
425 activate only the DUSP1 and 6 target MAPKs among the 43 tested kinases (Chan *et*
426 *al*, 2020; Kaltenmeier *et al*, 2017). Based on the response to kinase inhibitors and
427 anti-apoptotic antagonists, the cells that are HER2i resistant, but sensitive to DUSP6
428 inhibition, are co-dependent on PI3K/AKT, PLK1 and AXL kinase activities, and on
429 the anti-apoptotic proteins I kB, survivin, cIAP and/or XIAP (Figure EV4). Further
430 corroborating the role for DUSP6 as the anti-apoptotic target in stably HER2i
431 resistance cells, siRNA-mediated depletion of *DUSP6* induced apoptosis in MDA-
432 MB-453 cells (Fig. 4A). This was not seen with *DUSP1* inhibition (Fig. 4A). *DUSP6*
433 depletion also induced apoptosis in another HER2i resistant HER2+ cell line MDA-
434 MB-361 (Appendix Figure S4A). Furthermore, independent clones of CRISPR/CAS9
435 targeted MDA-MB-453 *DUSP6* KO cells showed impaired long-term colony growth
436 potential (Fig. 4B). This was due to loss of DUSP6 expression, as lentiviral re-
437 expression of DUSP6 rescued the phenotype (Appendix Figure S4B-E).

438

439 Notably, the genetic *DUSP6* targeting also sensitized MDA-MB-453 cells to several
440 HER2 targeting approaches. Indeed, whereas the parental MDA-MB-453 cells were
441 resistant to the clinically relevant concentrations of lapatinib, neratinib and
442 trastuzumab, this resistance was abrogated in the *DUSP6*-siRNA targeted cells (Fig.
443 4C, Appendix Figure S4F). These results also validate that *DUSP6* inhibition
444 sensitizes to HER2 inhibition regardless of whether small molecule inhibitors or
445 therapeutic antibody (trastuzumab) is used. The impact of genetic *DUSP6* targeting
446 in HER2i sensitization was recapitulated by BCI treatment (Fig. 4D). Additionally,
447 *DUSP6* depletion increased sensitivity to the combination of neratinib and
448 capecitabine (Fig. 4E), which is a combination therapy in clinical use (Saura *et al*,
449 2020). Furthermore, *DUSP6* depletion enhanced sensitivity to the combination of
450 tucatinib+trastuzumab+capecitabine (Appendix Figure S4G), which improves
451 progression free survival and overall survival in patients with HER2+ metastatic
452 breast cancer (Murthy *et al*, 2020).

453

454 Together with *DUSP6* overexpression experiments in HER2i sensitive cells (Fig. 3G-
455 I), these data provide strong evidence that *DUSP6* contributes to the HER2i
456 resistance both in monotherapy and combination therapy settings.

457

458 ***DUSP6* inhibition overcomes HER2 inhibitor resistance *in vivo***

459

460 To validate the *in vivo* relevance of the results, we used both genetic and
461 pharmacological targeting of *DUSP6* in HER2i resistant xenograft models. To start
462 with, we evaluated the impact of CRISPR/CAS9-mediated *DUSP6* knockout on the
463 xenograft growth of MDA-MB-453 cells in immunocompromised BALB/cOlaHsd-

464 Foxn1nu mice. Importantly, the two *DUSP6* KO clones showed significant and
465 indistinguishable antitumor effects as compared to the control cells (Fig. 5A). Next,
466 we asked whether pharmacological *DUSP6* blockade overcomes HER2i resistance
467 *in vivo*. For this purpose, we used two different HER2+ cell models, MDA-MB-453 or
468 HCC1954. When xenografts with these two cell lines had reached the approximate
469 size of 100 mm³, the mice were randomized into four treatment groups; vehicle,
470 lapatinib/neratinib (50 mg/kg), BCI (50 mg/kg), and lapatinib/neratinib+BCI.
471 Importantly, validating the *in vivo* HER2i resistance of both chosen HER2+ cell
472 models, tumors from both cell lines were fully resistant to clinically relevant doses of
473 either lapatinib or neratinib (Fig. 5B-E). Notably, both MDA-MB-453 and HCC1954
474 tumors also displayed strong resistance to BCI monotherapy (Fig. 5B-E), indicating
475 for tumor microenvironment-mediated impact as compared to the *in vitro* cultures.
476 However, combination of BCI very efficiently preempted the lapatinib or neratinib
477 resistance phenotype (Fig. 5B-E). Indicating for potential clinical utility, *DUSP6* and
478 HER2-targeted therapies displayed a clear synthetic lethal drug interaction when
479 assessed by a waterfall blot in both cell models (Fig. 5C, E). The dramatic
480 combinatorial activity of *DUSP6* and HER2 targeting on cellular viability was also
481 evidenced by lack of cytoplasmic eosin staining of the MDA-MB-453 xenograft tumor
482 after 24 d of treatment (Fig. 5F). Consistent with previous studies with BCI
483 (Kesarwani *et al.*, 2017; Ramkissoon *et al.*, 2019; Shojaee *et al.*, 2015; Wu *et al.*,
484 2018), we did not observe any apparent signs of toxicity or weight loss (Appendix
485 Figure S4D) in any treatment groups. In addition, normal fibroblasts displayed
486 several folds decreased sensitivity to BCI in an *in vitro* cell viability assay (Appendix
487 Figure S4E), further indicating for a favorable dose-window between impact of
488 *DUSP6* inhibition in HER2i resistance, and its effects to normal cells.

489

490 **DUSP6 targeting does not lead to the compensatory HER3 induction**
491 **characteristic to AKT inhibition**

492

493 Constitutive activity of PI3K/AKT signaling pathway is strongly associated with
494 HER2i therapy resistance (Berns *et al*, 2007; Majewski *et al*, 2015; Nagata *et al*,
495 2004). Further, clinical studies of HER2i plus PI3K/AKT inhibitors demonstrated
496 some clinical activity, but did not lead to approval of these combinations (Hudis *et al*,
497 2013; Saura *et al*, 2014). On the other hand, PI3K/AKT activation was one of the
498 DUSP6-driven hallmark gene sets associated with the DTP-DTEP transition (Fig. 1C
499 and 3F). Therefore, it was relevant to compare the quantitative and qualitative
500 differences between DUSP6 blockade versus AKT inhibition in combination with the
501 HER2i in the resistant models. Having demonstrated phenocopying growth effects
502 between genetic *DUSP6* inhibition and BCI, as well as resistance of *DUSP* KO cells
503 to BCI, these experiments were mostly performed by comparing the compounds
504 MK2206 (AKTi) and BCI (DUSP6i) as the alternative pharmacological HER2i
505 combination approaches.

506

507 In cell viability assay, both BCI and MK2206 synergized with already low micromolar
508 concentrations of lapatinib and neratinib in MDA-MB-453 and HCC1954 cells,
509 respectively (Fig. 6A,B, and Appendix Figures S4C and S5A). However, as
510 compared to AKT inhibition, DUSP6 targeting had qualitatively superior pro-apoptotic
511 activity. Regardless of efficient inhibition of AKT phosphorylation, MK2206 did not
512 induce apoptosis alone, or in combination with lapatinib (Fig. 6C,D). In contrast,

513 treatment with BCI plus lapatinib triggered apoptosis across all the tested cell models
514 (Fig. 6C,D, and Appendix Figure S5B).

515

516 HER3 is a key pro-survival receptor in HER2+ breast cancer cells (Haikala & Janne,
517 2021). Further, compensatory induction of HER3 is thought to be one of the primary
518 mechanisms behind the resistance to the combination of HER2 inhibition and AKT
519 targeting (Chandarlapaty *et al.*, 2011; Wilson *et al.*, 2012). Accordingly, AKT inhibition
520 resulted in HER3 induction in MDA-MBA-453 cells treated with either MK2206 alone,
521 and with MK2206-lapatinib combination (Fig. 6C,E). Pharmacological inhibition of the
522 AKT upstream kinase PI3K also induced HER3 expression (Appendix Figure S5C).

523 In contrast, BCI decreased HER2 and HER3 expressions as a monotherapy, and in
524 combination with lapatinib (Fig. 6C, F). Notably, both HER2 and HER3 were
525 downregulated 3 h already after BCI treatment, and this coincided with the induction
526 of ERK phosphorylation, and destabilization of DUSP6, both serving as signs for BCI
527 target engagement (Fig. 6G). Accordingly, siRNA-mediated knockdown of *DUSP6*
528 reduced HER2 and HER3 protein levels in MDA-MB-453, HCC1954, and the HER3+
529 triple negative breast cancer cell line MDA-MB-468 (Fig. 6H and Appendix Figures
530 S5D,E). Indicative of transcriptional regulation, *DUSP6* inhibition decreased *HER2*
531 and *HER3* mRNA expression, but did not impact HER2 and HER3 protein stability
532 (Appendix Figure S5F,G). Further, indicative of selective effects on HER2 and HER3
533 among the ERBB receptors, EGFR expression was unaffected by DUSP6 targeting
534 in MDA-MB-468 (Appendix Figure S5E). The tumor material from the BCI-treated
535 MDA-MB-453 xenograft model was further used for *in vivo* validation of HER3 as
536 DUSP6 downstream target. Indeed, BCI-treated tumors displayed vastly decreased
537 tumor cell immunopositivity for HER3, and to lesser extent HER2 (Fig. 6I). Finally,

538 clinically high *DUSP6* tumors had significantly higher expression of tyrosine 1298
539 phosphorylated HER3 (Fig. 6J).

540

541 These findings indicate that when HER2i is combined AKTi, the HER2+ cells survive
542 due to compensatory induction of HER3, whereas DUSP6 blockade rather inhibits
543 HER3, and therefore BCI+lapatinib treated cells succumb to apoptosis.

544

545 **DUSP6 targeting overcomes NRG-mediated HER2i therapy tolerance**

546

547 HER3 is activated in tumors by tumor microenvironment derived ligand NRG, and
548 NRG-activated HER3 drives HER2i tolerance (Kodack *et al*, 2017; Leung *et al*,
549 2015). On the other hand, our results indicate that DUSP6 may drive HER2i
550 resistance by promoting the expression of HER3. With this background, we
551 compared the capacity of DUSP6 and AKT inhibition to reverse HER2i tolerance by
552 the NRG/HER3 axis. As expected, (Kodack *et al.*, 2017; Leung *et al.*, 2015), NRG
553 treatment induced tolerance to both neratinib and lapatinib across all four tested
554 primarily sensitive cell lines (Fig. 7A and Appendix Figure S6A). The NRG-mediated
555 rescue from both HER2is was abrogated in a concentration dependent manner after
556 treatment with BCI, but not with MK2206 (Fig. 7A and Appendix Figure S6A). The
557 only exception was HCC2218 cells, in which also MK2206 reversed NRG-elicited
558 HER2i tolerance (Fig. 7A and Appendix Figure S6A). These results were validated at
559 the level of differential apoptosis induction between DUSP6 and AKT targeting.
560 Whereas NRG completely prevented HER2i-elicited induction of apoptosis in BT474
561 cells, and AKT inhibition could not reverse this, DUSP6 inhibition restored the
562 apoptotic activity (Fig. 7B). On the other hand, RNAi-mediated *HER3* knockdown

563 triggered apoptosis in MDA-MB-453 cells (Appendix Figure S6B). To functionally
564 prove that inhibition of *HER3* expression mediates BCI effects, we performed a
565 rescue experiment in MDA-MB-453 cells with ectopic stable overexpression of HER3
566 under heterologous CMV promoter (Appendix Figure S6C). As compared to control
567 cells, the HER3 overexpressing cells displayed significant resistance to BCI (Fig.
568 7C).

569

570 To link these results back to the development of HER2i tolerance, we found that
571 targeting of DUSP6, but not AKT, reversed the NRG-elicited effects on lapatinib
572 tolerance in the DTP assay (Fig. 7D). This BCI effect was likely due to DUSP6
573 inhibition, as siRNA-mediated *DUSP6* depletion also abrogated the NRG-induced
574 cell survival in BT474 cells (Appendix Figure S6D). Importantly, deregulation of
575 NRG-ERBB axis was evidenced also during the DTP-DTEP transition of lapatinib
576 treated cells as, concomitantly with *DUSP6* regulation (Fig. 2C), *NRG3* and *ERBB4*
577 were found upregulated in DTEP versus DTP cells (Appendix Figure S6E). Further,
578 providing clinical validation for the link between NRG and DUSP6, *NRG* mRNA was
579 significantly overexpressed in breast tumors with high *DUSP6* mRNA expression
580 (Fig. 7E).

581

582 Due to brain microenvironment derived NRG, HER3 has a key role in brain
583 metastatic growth of HER2+ breast cancers (Da Silva *et al*, 2010; Haikala & Janne,
584 2021). Based on the newly discovered role for DUSP6 in promoting HER3
585 expression, we investigated contribution of DUSP6 in the brain metastatic outgrowth
586 by using GFP-positive MDA-MB-361 cells as yet additional HER2+ *in vivo* model. To
587 this end, we quantitated the zebrafish intracranial tumor area derived from GFP+

588 MDA-MB-361 cells transfected prior tumor implantation either with control or *DUSP6*
589 targeting siRNA. As shown in Fig. 7F, the zebrafish larva with *DUSP6* targeted cells
590 had significantly smaller tumors 3d after the intracranial injection. Further, mice
591 bearing the intracranial *DUSP6* KO MDA-MB-453 tumors had a significantly longer
592 survival time as compared with the CAS9 control group (Fig. 7G).

593

594 Collectively these results demonstrate that DUSP6 inhibition is superior to AKT
595 blockade as a HER2i combination therapy strategy due to its newly discovered
596 capacity to inhibit the NRG-HER3 axis and has potential in inhibiting brain metastatic
597 growth of HER2+ cells.

598

599 **A DUSP6-HER3 feed forward loop drives the HER2i tolerance**

600

601 After identifying previously unrecognized regulation of HER3 by DUSP6 and
602 demonstrating its functional relevance, we asked whether the HER3 reciprocally
603 regulates DUSP6 expression. Indeed, *DUSP6* mRNA expression was potently
604 inhibited already with the smallest tested concentration of neratinib or lapatinib in the
605 HER2i sensitive cells (BT474, BT474Br) (Fig. 8A and Appendix Figure S7A; in
606 green). However, among the HER2i resistant cell lines, *DUSP6* was not inhibited by
607 HER2is in MDA-MB-361, MDA-MB-453, BT474Br-LR, and BT474-LR cells, whereas
608 HCC1954 showed an intermediate phenotype (Fig. 8A and Appendix Figure S7A; in
609 red). Additionally, this regulation was specific to *DUSP6*, as *DUSP1* mRNA
610 expression was not inhibited by HER2 targeting in any of the tested cell modes (Fig.
611 8A and Appendix Figure S7A). Clinically *DUSP6* and *HER3* mRNA expression also
612 correlated in HER2+ cancer samples in the TCGA-BRCA dataset (Cerami *et al.*,
613 2012)(Appendix Figure S7B). Differential regulation of DUSP6 expression by HER2i

614 in sensitive (BT474Br, BT474) versus resistant (MDA-MB-361, MDA-MB-453,
615 BT474BrLR) cells was validated at the protein level by western blotting (Fig. 8B,C
616 and Figure EV5). Importantly, RNAi-mediated knockdown of *HER3* decreased
617 DUSP6 expression (Fig. 8D). *HER3* dependent DUSP6 regulation was further
618 supported by induction of *DUSP6* mRNA and protein expression by treatment of
619 serum-starved BT474 or BT474Br cells with the *HER3* ligand NRG (Fig. 8E, F and
620 Appendix Figures S7C,D). Induction of DUSP6 was selective for NRG, since
621 hepatocyte growth factor (HGF), which activates MET RTK, failed to increase
622 DUSP6 in BT474 cells (Appendix Figure S7C,D). To gain insights into the
623 mechanism by which *HER3* regulates DUSP6, the NRG treated cells were co-treated
624 either with AKTi MK2206, or the MEK1/2 inhibitor trametinib. Consistent with a
625 previous report that DUSP6 is a transcriptional ERK1/2 target (Zandi *et al.*, 2022),
626 treatment with trametinib inhibited both ERK phosphorylation and DUSP6 expression
627 in all tested cell lines (Fig. 8E-G and Appendix Figure S7E), whereas AKT inhibition
628 by MK2206 further increased DUSP6 expression (Fig. 8E-G). Notably, HER2i-
629 elicited inhibition of DUSP6 expression correlated with the capability of HER2i to
630 impact ERK phosphorylation (Fig. 8F, G and Figure EV5A,B).

631

632 Collectively these results reveal that inhibition of the newly discovered DUSP6-*HER3*
633 feed-forward loop has a major contribution to HER2i therapy response, and that lack
634 of DUSP6 inhibition is a novel HER2i resistance mechanism in acquired resistant
635 cells in which HER2i fails to target MEK activity (Fig. 8H).

636
637

638 **Discussion**

639

640 Cancer therapy resistance is initiated by non-genetic signaling rewiring resulting in
641 major changes in the epigenetic and transcriptional landscapes of DTPs (Chang *et*
642 *al.*, 2022; De Conti *et al.*, 2021; Marine *et al.*, 2020; Sharma *et al.*, 2010). It is
643 commonly believed that transition from dormant DTPs to proliferating DTEPs is a
644 pivotal step towards development of the disseminated disease, and eventually late-
645 stage genetic changes which determine the ultimate therapy resistance (Aguirre-
646 Ghiso, 2021; Marine *et al.*, 2020). Here, we report the first transcriptomic analysis of
647 the DTP-DTEP transition in TKI treated cancer cells. In addition to importance of the
648 discovery of the role of DUSP6 in DTP-DTEP transition, the transcriptome data will
649 provide a rich resource for future studies to understand different stages of the HER2i
650 resistance development. Based on the fuzzy clustering data (Appendix figure S1 and
651 Dataset EV2), the gene clusters 1, 2 and 6, contain genes that are strongly regulated
652 upon the DTP-DTEP transition and are therefore contain many additional genes
653 involved in the evasion of the DTP cells from lapatinib-induced growth inhibition. The
654 longitudinal transcriptomics profiles also allowed us to identify potential master
655 transcription factors involved in the lapatinib resistance development. The functional
656 relevance of the differentially expressed genes associated with each therapy
657 tolerance transition obviously need to be validated in future studies stemming from
658 this novel resource. Further, to understand therapy tolerance development
659 projectories at the single cell level, similar studies are needed by employing single
660 cell RNA sequencing technologies.

661

662 Phosphatases have recently emerged as novel druggable targets for cancer therapy
663 (Lazo *et al.*, 2018; Vainonen *et al.*, 2021; Zandi *et al.*, 2022). However, their
664 contribution to development of non-genetic TKI therapy tolerance is still poorly
665 understood. In the present study, we asked which phosphatases might contribute to
666 the development of HER2i tolerance and resistance and explored their potential role
667 as therapy targets in combination with the HER2i therapies in HER2+ breast cancer.
668 Via transcriptomics analysis of lapatinib tolerance development over six months, we
669 discovered an important role for DUSP6 in the re-growth of HER2i tolerant cells and
670 showed that its genetic and pharmacological blockade potentiates HER2i sensitivity
671 *in vitro* and *in vivo* in multiple different HER2+ cell models. Mechanistically, we
672 discovered that transcriptional *DUSP6* inhibition is an important contributor to
673 effective HER2i response whereas the lack of HER2i-elicited *DUSP6* inhibition in the
674 resistant cells provides a novel explanation for drug resistance in these cells (Fig.
675 8H). We further discovered DUSP6 as a novel activator of *HER3* expression and
676 demonstrated that *HER3* inhibition is a prerequisite for the therapeutic impact of
677 DUSP6 inhibition. Inhibition of *HER3* by DUSP6 targeting appears also an important
678 mechanistic explanation for the superior apoptotic activity as compared to PI3K/AKT
679 targeting in combination with HER2i. As we demonstrate, the therapeutic impact of
680 DUSP6 targeting is not compromised by the NRG-mediated feedback to *HER3* as is
681 the case with AKT targeting and thereby our data identify DUSP6 targeting as a
682 novel approach to target NRG-*HER3* axis to overcome HER2i resistance. These are
683 important advantages favoring DUSP6 blockade versus AKT inhibition as a future
684 strategy for treatment of HER2+ breast cancer. A particularly important translational
685 finding in our study is that DUSP6 defines therapy sensitivity of the lapatinib resistant
686 cells in response to several ERBB TKIs with different specificities, and to their

687 chemotherapy combinations. This is consistent with the proposed HER3-DUSP6
688 positive feedback mechanism, as HER3 or NRG overexpression confer resistance to
689 several cancer drugs (Erjala *et al.*, 2006; Haikala & Janne, 2021; Knuefermann *et*
690 *al.*, 2003; Recondo *et al.*, 2020; Wilson *et al.*, 2012; Yonesaka *et al.*, 2011). Thereby
691 identification of DUSP6 targeting as a novel approach for HER3 inhibition may have
692 broad ramifications in different combination therapy settings across different cancer
693 types. HER2 and 3 play also essential roles in the development of brain metastasis
694 which causes death of more than 30% of stage IV HER2+ breast cancer patients
695 (Berghoff *et al.*, 2014; Da Silva *et al.*, 2010; Fecchi *et al.*, 2019). To this end, DUSP6-
696 mediated regulation of HER2 and 3 suggested that its inhibition may retard
697 development of brain metastasis. Indeed, our findings directly support these
698 conclusions as *DUSP6* knockout in tumor cells improves survival of mice with
699 intracranial HER2+ tumors and the outgrowth of HER2+ breast tumor cells in a
700 zebrafish intracranial model. Linking our results further to future therapy of HER2+
701 brain metastasis, we showed that *DUSP6* knockdown increases sensitivity to
702 tucatinib+trastuzumab+capecitabine combination regimen, which show significant
703 clinical activity in HER2+ breast cancer patients with brain metastasis (Murthy *et al.*,
704 2020).

705

706 While demonstrated here for the first time in the context of HER2i therapy resistance,
707 genetic DUSP6 inhibition has recently been shown to inhibit malignant phenotypes in
708 other cancer types (Shojaee *et al.*, 2015; Wu *et al.*, 2018; Zandi *et al.*, 2022).
709 Consistent with these reports, genetic inhibition of *DUSP6* in our study resulted in
710 significant inhibition of HER2+ breast cancer cell viability, HER2i resistance, colony
711 forming potential, and *in vivo* tumor growth. Mechanistically, DUSP6 inhibition

712 converted cytostatic response to HER2i to an apoptotic response, which is
713 considered as a paramount for cancer therapy strategies aiming for cancer cure. On
714 the other hand, overexpression of DUSP6 converted HER2i sensitive cells to
715 resistant in both cell viability and apoptosis assays. Importantly, all our main
716 conclusions remained valid regardless of whether DUSP6 was inhibited either by
717 siRNA, CRISPR/CAS9, or by pharmacological inhibitors BCI and BCI-215. We
718 further demonstrated nearly immediate target engagement, as well as resistance of
719 three independent *DUSP6* knock-out clones to BCI-elicited cell viability inhibition.
720 Therefore, together with recent results from the others (Kong *et al.*, 2023; Shojaee *et*
721 *al.*, 2015), we are confident that the results achieved by BCI and BCI-215 are
722 dependent on their inhibitory effects on DUSP6 despite a recent report questioned
723 their selectivity using other cellular system (Thompson *et al.*, 2022).

724

725 The results identified DUSP6 as a novel combination therapy target with existing
726 clinical HER2 targeting strategies including both small molecule and antibody
727 mediated HER2 inhibition and chemotherapy combinations. In that regard, our
728 xenograft results demonstrate significant potential for pharmacological DUSP6
729 inhibition in overcoming HER2i resistance *in vivo* by using two different HER2i
730 resistant cell lines, and two different HER2is. Whereas neither HER2 nor DUSP6
731 inhibition alone did not have therapeutic effect on tumors, the combination showed
732 very potent synthetic lethal phenotype further validating our *in vitro* results. The lack
733 of monotherapy effect of BCI, combined with clear evidence for downstream target
734 mechanism engagement *in vivo* also alleviates concerns about overall cellular
735 toxicity behind the BCI-elicited HER2i synergy. This is consistent with previous
736 findings demonstrating antitumor effects with BCI and BCI-215 without obvious

737 systemic toxicity in *in vivo* models of gastric cancer, leukemia, and malignant
738 peripheral nerve sheath tumor (Kesarwani *et al.*, 2017; Ramkissoon *et al.*, 2019;
739 Shojaee *et al.*, 2015; Wu *et al.*, 2018).

740

741 In summary, we provide first transcriptional map of DTP-DTEP transition under TKI
742 tolerance development in cancer. The results specifically identify DUSP6 targeting
743 as a novel approach to target HER3-mediated ERBB TKI resistance. Ultimately, the
744 work provides proof-of-principle evidence to encourage development of next
745 generation DUSP6 inhibitors (with brain penetrance) to test the clinical relevance of
746 the presented therapy scenarios.

747

748 **Materials and Methods**

749

750 **Reagents**

751 Tissue culture reagents including regular RPMI, DMEM, RPMI and FBS were
752 purchased from Sigma. The recombinant NRG, HGF and β-estradiol (E2) were from
753 Peprotech. BCI was purchased from Axon Medchem. BCI-215 was provided by Dr.
754 Andreas Vogt, University of Pittsburgh Drug Discovery Institute, Pittsburgh, PA,
755 USA. The HER2 inhibitors and the other compounds used in the drug screening
756 were purchased from Adooq Bioscience. All the agents were dissolved in DMSO and
757 the final concentration of DMSO did not exceed 0.1% [v/v] in all the treatments.

758 **Cloning and plasmids**

759 pBABE-puro-gateway-ERBB2 was a gift from Matthew Meyerson (Addgene plasmid
760 No. 40978; <http://n2t.net/addgene:40978>; RRID:Addgene_40978). ERBB3 wild-type
761 was cloned from pBABE-puro-gateway-ERBB3 (Koivu *et al.*, 2021) into pLenti CMV
762 Puro DEST (w118-1), a gift from Eric Campeau and Paul Kaufman (Addgene
763 plasmid # 17452;<http://n2t.net/addgene:17452> ; RRID:Addgene_17452) through
764 Gateway cloning (Chakroborty *et al.*, 2019) to create pLenti-CMV-Puro-ERBB3. The
765 DUSP6 plasmid was purchased from Addgene (#27975) and the Kinase interaction
766 motif (KIM) mutants were prepared by site directed mutagenesis (GenScript Inc)
767 generating R64A, R65A double mutant defective in ERK binding as described
768 (Nichols *et al.*, 2000).

769 **Generation of stable lines**

770 To overexpress wild-type ERBB2, pBABE-puro-gateway-ERBB2 was transfected
771 (using Fugene6 transfection reagent; Promega Catalog # E2692) into amphotropic
772 Phoenix HEK293T cells (a gift from Dr. Garry Nolan) to generate retroviruses, which
773 were used to transduce MDA-MB-453, as described previously (Chakroborty *et al.*,

774 2019). pLenti-CMV-Puro-ERBB3 was co-transfected with virus-packaging plasmids
775 pMLDg/pRRE (addgene #12251), pMD2.G (addgene #12259), and pRSV-Rev
776 (addgene #12253) into HEK293T cells using Fugene6 transfection reagent to
777 produce lentiviruses. The lentivirus-containing supernatant was used to transduce
778 MDA-MB-453 to over-express wild-type ERBB3. After viral transduction cells were
779 treated with 1 µg/mL puromycin (Gibco) for 48 h to select the cells with stable
780 expression of the respective introduced transgenes.

781 For DUSP1 and 6 overexpression, lentiviral particles containing full length of either
782 DUSP1 (Genecopoeia), DUSP6 (Addgene #27975), or control empty (Genecopoeia)
783 vector were generated in HEK293FT packaging cell line (complete medium: high
784 glucose DMEM, 10% FBS, 0,1mM NEAA, 1mM MEM Sodium Pyruvate, 6mM L-
785 Glutamine, 1% Pen/Strep and 0,5mg/ml Geneticin) by transient transfection of
786 transfer vector 2nd generation packaging plasmid-psPAX2 (Addgene #12259) and
787 envelope vector-pMD2 (Addgene #12260) with the ratio (7:2:1) using calcium-
788 phosphate precipitation method. Seventy-two hours post-transfection medium
789 containing viral vectors was collected, concentrated for 2 h by ultracentrifugation in
790 swing-out rotor SW-32Ti (Beckman Coulter), 26,000g, resuspended in residual
791 medium and flash-frozen in liquid nitrogen. Functional titer ~1x10⁸ was measured in
792 HEK293FT cells and FACS (BD LSRII Fortessa, Becton Dickinson). To obtain stable
793 overexpression of DUSP1, DUSP6 or double DUSP1+6 population on day zero,
794 8x10⁴ cells were seeded in a 24-well plate. 24 h later, the cells were transduced with
795 MOI 60 of lentiviral stocks in a low volume of full media. Medium containing viral
796 particles was removed 16 h later. Cells expressing DUSP1 and GFP indicative of
797 lentiviral integration were collected by fluorescence assisted cell sorting (BD
798 FACStar II cell sorter, Becton Dickinson). FACS gating was set at 10% top high

799 fluorescence signal. DUSP6 transduced BT474 cells were selected with 3 µg/mL of
800 puromycin. DUSP1 and 6 expressing cells were obtained by sequential transduction
801 (MOI 2, 6, 10), puromycin selection and later GFP fluorescence assisted cell sorting
802 (BD FACSaria II cell sorter, Becton Dickinson). The levels of protein were confirmed
803 by Western blot analysis.

804 For stable overexpression of DUSP6 and DUSP6 KIM mutant, DUSP6
805 (Addgene #27975) and DUSP6^{R64-65A} lentiviral vectors were co-transfected with
806 virus-packaging plasmids pMLDg/pRRE, (Addgene #12251), pMD2.G (Addgene
807 #12259), and pRSV-Rev (Addgene #12253) into HEK293T cells using FuGene6
808 transfection reagent to produce lentiviruses. 48 h after transfection viral supernatants
809 were collected, filtered, and added to pre-plated BT474 cells along with 10 µg/mL
810 polybrene. Transduced cells were selected with 2 µg/mL puromycin, and the protein
811 levels were confirmed by Western blot analysis.

812 To rescue the DUSP6 KO MDA-MB-453 clones, the pLEX307-hygro-DUSP6
813 lentiviral vector was co-transfected with virus-packaging plasmids pMLDg/pRRE,
814 (Addgene #12251), pMD2.G (Addgene #12259), and pRSV-Rev (Addgene #12253)
815 into HEK293T cells using FuGENE6 transfection reagent. 48 hours after transfection
816 viral supernatants were collected, filtered, and added to MDA-MB-453 DUSP6 KO
817 cells (g1, clone 22) along with 10 µg/mL polybrene. Transduced cells were selected
818 with hygromycin (250µg/ml).The MDA-MB-453 CAS9 control, DUSP6 KO, and
819 DUSP6 transduced KO cells were seeded at low density and maintained for 10 d.
820 The colonies were stained with 0.5% crystal violet in methanol and imaged using an
821 Epson scanner. Colony quantification was done by using the ImageJ ColonyArea
822 plugin.

823

824 **FACS**

825 MDA-MB-453 cells transduced with lentiviruses encoding wild-type ERBB3 were
826 washed with azide-free PBS, trypsinized and suspended in ice-cold sorting buffer
827 (PBS +1% Goat serum, Life technologies catalog # PCN5000). The cells were
828 incubated with anti-ERBB3 (MAB3481, R&D systems) for 1 h on ice, and with anti-
829 mouse Alexa Fluor 405 (A-31553, Invitrogen) for 30 min on ice in a dark
830 environment. Single cell suspension was analyzed and sorted on Sony SH800 Cell
831 Sorter to select cell-pools with high surface ERBB3 expression.

832 **CRISPR/CAS9 knockout system**

833 A two-component CRISPR system was used to generate *DUSP6* KO cells (Adli,
834 2018). *DUSP6* sgRNAs (seq#1- CATCGAGTCGGCCATCAACG, seq#2-
835 GACTGGAACGAGAATACGGG, seq#3- CCATGATAGATACTGCTCAGA) were
836 selected using DeskGEN platform and cloned according to F. Zhang lab protocol.
837 Separate lentivectors containing spCas9 (lentiCas9-Blast a gift from Feng Zhang
838 (Addgene plasmid # 52962) and sgRNA (lentiGuide-Puro a gift from Feng Zhang
839 (Addgene plasmid # 52963) were produced in HEK293FT packaging cell line by
840 transient cotransfection. Shortly, 40-70% confluent HEK293FT cells were used for
841 transfections with 14 µg of transfer vector, 4 µg of packaging vector psPAX2 (gift
842 from Didier Trono (Addgene plasmid # 12260), 2 µg envelope vector pMD2.G (gift
843 from Didier Trono (Addgene plasmid # 12259) mixed in 0.45 mL water, 2.5M CaCl₂,
844 and 2x HeBS (274 mM NaCl, 10 mM KCl, 1.4 mM Na₂HPO₄, 15 mM D-glucose, 42
845 mM Hepes, pH 7.06) per 10 cm dish. Before adding to the cells, the DNA-HeBS mix
846 was incubated for 30 min at room temperature. After overnight incubation medium
847 with DNA precipitate was gently removed from the cells and replaced with a full fresh
848 medium. Media containing viral particles was collected after 72 h, spun at 300 rpm

849 for 5 min at room temperature to remove cell debris, filtered through 0.45 µm PES
850 filter, and concentrated by ultracentrifugation for 2 hours at 25,000rpm, 4°C
851 (Beckman Coulter). The pellet containing lentiviral particles was suspended in the
852 residual medium, incubated for ~2 hours in +4°C with occasional mild vortex,
853 aliquoted, snap-frozen and stored in -70°C. P24 ELISA measured physical lentiviral
854 titer with a serial dilution of virus stock according to manufacturer protocol.

855 To generate DUSP6KO clones in MDA-MB-453, 1e+05 cells were seeded on a 24-
856 well plate. The next day the cells were transduced with Lenti-Cas9 (MOI 1, 5, 10),
857 and 72 h later, 8 µg/mL of Blasticidin was applied to select only Cas9 expressing
858 cells. Cells transduced with the smallest number of Lenti-Cas9 particles that survived
859 after the parallel control well was cleared proceeded to the next step. In the second
860 stage, the mixed pool of stably expressing Cas9 cells was transduced with Lenti
861 sgRNA vectors (MOI 5,10,15,20), and 72 h later, 1 µg/uL Puromycin was applied on
862 the cells to select double-positive Cas9+/Lenti sgRNA+ cells. Based on Western blot
863 results, cell populations showing the highest reduction in DUSP6 protein levels were
864 single sorted (Sony SH800 cell sorter, Sony Biotechnology Inc) and re-grown into a
865 clonal cell population. On average, about 20 clones per sgRNA population were
866 screened using Western blotting and qPCR. Sanger sequencing was used to confirm
867 full knockout status.

868 **Cell Culture and Transfections**

869 All cell lines were purchased from the American Type Culture Collection (ATCC) and
870 were maintained at 37 °C and 5% CO₂ in a humidified incubator and cultured
871 according to the ATCC recommendations. Cell line authentication was performed by
872 STR profiling and using Cell ID™ system (Promega). The cultures were routinely
873 tested for mycoplasma contamination. The information about siRNAs for *DUSP1*,

874 *DUSP6*, *HER2*, *HER3*, *AKT1* and negative control siRNAs are in Table EV1.
875 Transient transfections were performed with lipofectamine RNAiMAX reagent
876 (ThermoFisher) according to the manufacturer's instructions.

877 **Cell growth assays**

878 The cells were seeded at a density of 2×10^3 into 96-well plates and treated with
879 increasing concentrations of the drugs for 48 h. Cell viability was determined using
880 WST-1 assay (Sigma). Vehicle-treated cells were used as the control group. For the
881 clonogenic survival assay, cells were seeded in 6-well plates at a density of 1000
882 cells/well. After 24 h, the media was changed, and the cells were maintained for
883 another 10 d. The resulting colonies were stained/fixed with 0.5% crystal violet
884 imaged using an inverted microscope.

885 To yield DTPs in NSCLC, melanoma and colorectal cancer cell lines, the following
886 treatments were carried out: NSCLC cell line HCC827, melanoma cell line A375, and
887 colorectal cancer HT-29 cell line were cultured under standard conditions. The
888 following treatments were applied for 10 d: HCC827, 1 μ M osimertinib; A375, 1 μ M
889 dabrafenib+100 nM trametinib; HT-29, 1 μ M dabrafenib+10 μ g/ml cetuximab.

890 **Drug combination analysis**

891 To explore the efficacy of drug combinations, growth inhibition was determined by
892 WST-1 assay and the results were evaluated by Bliss SynergyFinder (Ianevski *et al*,
893 2017). Visualization of synergy scores is depicted as a synergy map. An average
894 synergy score of 0 is considered additive, less than 0 as antagonistic and over 0 as a
895 synergistic outcome.

896 **Caspase 3/7 activity assay**

897 The Caspase-Glo® 3/7 Assay System (Promega), a luminescence-based assay for
898 detection of active caspase-3 and 7, was used to quantitatively determine apoptotic

899 cell death. Following caspase cleavage of the proluciferin DEVD substrate, a
900 substrate for luciferase is released and results in luciferase reaction and production
901 of light.

902 **Western blot analysis**

903 The cells were lysed for 30 min in ice-cold RIPA buffer (50 mM Tris-HCl, pH 8.0, 150
904 mM NaCl, 1.0% NP-40, 0.5% sodium deoxycholate and 0.1% SDS) containing
905 protease and phosphatase inhibitors (ThermoFisher). The assay was performed with
906 primary and Licor secondary antibodies (Licor Biosciences). β-actin was used as the
907 loading control. The list of antibodies is in Table EV2.

908 **Analysis of gene expression by quantitative reverse transcription-PCR**

909 Quantitative reverse transcription-PCR (qRT-PCR) analysis was done on a
910 QuantStudio Real-Time PCR instrument (ThermoFisher) using PowerUp™ SYBR®
911 Green Master Mix (ThermoFisher). The primer sequences are listed in Table EV3.
912 The target gene expression levels were normalized to beta-2-microglobulin (*B2M*)
913 levels. For calculations, $2^{-\Delta\Delta CT}$ formula was used, with $\Delta\Delta CT = (CT_{Target} - CT_{B2M})$
914 experimental sample – $(CT_{Target} - CT_{B2M})$ control samples, where CT is the cycle
915 threshold.

916 **Animal studies**

917 The animal experiments were performed according to the Animal Experiment Board
918 in Finland (ELLA) for the care and use of animals under the licenses
919 4161/04.10.07/2015 and 9241/2018. The animals were kept under pathogen-free
920 conditions in individually ventilated cages in an animal care facility. Mice were kept
921 on a 12 h light/dark cycle with access to autoclaved water and irradiated chow *ad*
922 *libitum* and were allowed to adapt to the facility for 1 week before starting the
923 experiments. For the subcutaneous experiments, MDA-MB-453 (5×10^6) and

924 HCC1954 (3×10^6) cells were injected into the right flank of six- to eight-week-old
925 BALB/cOlaHsd-Foxn1nu mice (Envigo, France). Mice with tumor size $\sim 100 \text{ mm}^3$
926 were randomized into experimental and control groups. Tumor dimensions were
927 measured with Vernier calipers and tumor volume were calculated as 1/2 larger
928 diameter x (smaller diameter) 2 . For the intracranial model, 1×10^5 cells in 5 μL of
929 PBS were inoculated into the brain of anaesthetized mice. The mice were then
930 imaged with bioluminescence and based on the bioluminescence signal were
931 randomized to experimental and control groups, as described earlier (Merisaari *et al*,
932 2020). Mice were euthanized when they became moribund when they reached
933 defined study end points.

934 **Zebrafish studies**

935 Zebrafish embryo xenograft studies were performed under the license
936 ESAVI/9339/04.10.07/2016 (National Animal Experimentation Board, Regional State
937 Administrative Agency for Southern Finland). Briefly, the *DUSP6* knockdown GFP-
938 MDA-MB-361 cells were injected into the brain of zebrafish embryos from the dorsal
939 side. One day after injection (1 dpi), successfully transplanted embryos were placed
940 in CellView glass bottom 96-well plate (1 embryo/well) and embryos were incubated
941 in E3 + PTU at 33 °C. The xenografted embryos were imaged using a Nikon Eclipse
942 Ti2 fluorescence microscope and a 2x Nikon Plan-Apochromat (NA 0.06) objective.
943 Each embryo was imaged at 1dpi and 4dpi using brightfield illumination and a GFP
944 fluorescence filter set (excitation with 470nm LED). Each image was inspected
945 manually to filter out severely malformed, dead or out of focus embryos. The tumor
946 area was measured using ImageJ (NIH). The fold change in tumor size was
947 calculated as follows: GFP intensity (4dpi)/GFP intensity (1dpi)

948 **RNA-sequencing**

949 RNA-sequencing was conducted at the Finnish Functional Genomic Center, The
950 University of Turku, Finland. RNA was harvested using the NucleoSpin RNA
951 purification kit (Macherey-Nagel), followed by treatment with DNase to remove
952 genomic DNA. RNA (300 ng) was reverse transcribed using the Illumina TruSeq
953 Stranded Total mRNA kit. The quality of the samples was ensured using Agilent
954 Bioanalyzer 2100 or Advanced Analytical Fragment Analyzer. Sample concentration
955 was measured with Qubit® Fluorometric Quantitation (Life Technologies) and/or
956 KAPA Library Quantification kit for Illumina platform, KAPA Biosystems. Sequencing
957 run was performed using the Illumina NovaSeq 6000 instrument. Genomic alignment
958 was performed using Rsubread v. 2.0.0 and the reads were mapped to the human
959 reference genome hg38. Aligned reads were assigned to RefSeq gene models using
960 the same R package with its default settings.

961 Differentially expressed genes and pathways were identified using the R package
962 limma. Latest hallmark gene sets were downloaded from the Molecular Signatures
963 Database version 7.4 (<http://www.gsea-msigdb.org/gsea/msigdb/index.jsp>) and used
964 within Gene Set Variation Analysis (GSVA) allowing pathway enrichment estimates
965 for each sample (Hanzelmann *et al*, 2013). Data was transformed using log(x+1)
966 after normalization and the RNA-sequencing pipeline run. Heatmaps were plotted
967 using the ComplexHeatmap package (Gu *et al*, 2016). R statistical software version
968 4.0.3 was used for the statistical analyses and visualizations.

969 **cBioPortal database analyses**

970 The correlation analysis between gene expression and breast cancer subtypes was
971 examined using the METABRIC breast cancer cohort with PAM50 classification
972 (Pereira *et al.*, 2016), TCGA breast invasive carcinoma dataset and the TCGA
973 Firehose legacy dataset (Gao *et al.*, 2013). The RNA-seq data from breast invasive

974 carcinoma samples and the relevant clinical information are available at the TCGA
975 data portal, cBioPortal for Cancer Genomics (<http://www.cbioportal.org/>). According
976 to the PAM50 classification, METABRIC breast cancer patients were divided into 5
977 subtypes, including the basal (n=199), HER2+(n=220), Lum A (n=679), Lum B
978 (n=461) and Normal-like (n=140). ER and HER2 status were assessed using the
979 patient's IHC information. The survival outcomes were extracted from the TCGA
980 breast invasive carcinoma dataset.

981 For multivariable Cox regression analyses, N=121 HER2+ patients from the TCGA-
982 BRCA cohort were extracted, with reported pathological T-stages and lymph node
983 statuses included as clinical factors and relapse free survival modelled as the end-
984 point. Further, transcriptomics was included as log2-transformed values for RSEM
985 normalized expression of DUSP6.

986 **Transcription factor binding analyses**

987 To predict transcription factors enriched in the significantly differentially regulated
988 genes during the therapy tolerance transitions we used ChEA3: transcription factor
989 enrichment analysis by orthogonal omics integration tool (Keenan *et al*, 2019).
990 Differentially regulated genes were provided as input to the tool and the significantly
991 associated transcription factors were obtained using ENCODE (Encyclopedia of
992 DNA Elements) ChIP-seq library. The output file consists of a list of transcription
993 factors arranged based on a scaled rank where a lower value means a higher
994 significance in the gene list. An FDR value < 0.05 was considered significant.

995 To predict the transcription factors binding the DUSP6 promotor region, Cistrome DB
996 Toolkit was used (Zheng *et al*, 2019). As an input 4000 base pairs upstream of the
997 DUSP6 gene were entered in the Cistrome DB Toolkit. This provided a list of

998 transcription factors based on the regulatory potential (RP score) derived by
999 comparing the CHIP-seq data sets.

1000 **Statistical analysis**

1001 Differentially expressed genes and pathways were identified using the R package
1002 limma (Ritchie *et al.*, 2015). Latest hallmark gene sets were downloaded from the
1003 Molecular Signatures Database version 7.4 ([http://www.gsea-](http://www.gsea-msigdb.org/gsea/msigdb/index.jsp)
1004 [msigdb.org/gsea/msigdb/index.jsp](http://www.gsea-msigdb.org/gsea/msigdb/index.jsp)) and used within Gene Set Variation Analysis
1005 (GSVA) allowing pathway enrichment estimates for each sample (Hanzelmann *et al.*,
1006 2013), with FDR-cutoff <0.25 used for the pathway enrichment analyses. Data was
1007 transformed using $\log(x+1)$ after normalization and the RNA-sequencing pipeline
1008 run. Heatmaps were plotted using the ComplexHeatmap package (Gu *et al.*, 2016).
1009 R statistical software (R Core Team (2023). R: A language and environment for
1010 statistical computing. R Foundation for Statistical Computing, Vienna, Austria. URL:
1011 <https://www.R-project.org>) version 4.0.3 was used for the statistical analyses and
1012 visualizations.

1013 All data were evaluated in triplicate against the vehicle-treated control cells and
1014 collected from three independent experiments. In addition to R analyses, data were
1015 visualized and analyzed using GraphPad Prism 8.3.0 using one-way ANOVA and the
1016 unpaired two-tailed student's *t* test. All such data are presented as mean \pm standard
1017 deviation (SD).

1018 **Data Availability**

1019 The gene expression data from this publication have been deposited to the GEO
1020 database (<https://www.ncbi.nlm.nih.gov/geo/>) and assigned the identifier
1021 GSE231526 (<https://www.ncbi.nlm.nih.gov/geo/query/acc.cgi?acc=GSE231526>).

1022

1023 **Disclosure and competing interests statement**

1024

1025 The authors declare no competing interests.

1026

1027

1028 **Author contributions**

1029 **Majid Momeny:** Conceptualization; Validation; Supervision; Visualization; Writing;

1030 Investigation; Formal analysis; Methodology. **Mari Tienhaara:** Validation;

1031 Investigation; Methodology. **Mukund Sharma:** Validation; Investigation;

1032 Methodology. **Deepankar Chakroborty:** Methodology. **Roosa Varjus:** Formal

1033 analysis. **Iina Takala:** Methodology. **Joni Merisaari:** Methodology. **Artur Padzik:**

1034 Methodology; Validation. **Andreas Vogt:** Methodology. **Iikka Paatero:** Methodology;

1035 Validation. **Klaus Elenius:** Supervision; Methodology. **Teemu D. Laajala:**

1036 Methodology; Formal analysis. **Kari J. Kurppa:** Supervision; Investigation;

1037 Methodology. **Jukka Westermarck:** Conceptualization; Supervision; Validation;

1038 Project administration; Writing-review and editing.

1039 **Acknowledgement**

1040 Taina Kalevo-Mattila is acknowledged for superior technical support and the entire

1041 Turku Bioscience Centre personnel is thanked for excellent working environment.

1042 We acknowledge Zhong-Yin Zhang for PRL1i compound, Norma O'Donovan,

1043 National Institute for Cellular Biotechnology, Dublin City University, Ireland, for some

1044 HER2+ breast cancer cell lines used in this study, and Dihua Yu, The University of

1045 Texas MD Anderson Cancer Center, USA, for the BT474Br cells. We further

1046 acknowledge important contributions of the following core facilities of Turku

1047 Bioscience Centre (University of Turku and Åbo Akademi University) supported by

1048 Biocentre Finland: Finnish Functional Genomics Center, Screening unit, and

1049 Zebrafish unit. This study was supported by funding from Finnish Cancer

1050 Associations (JW), Foundation of Finnish Cancer Institute (MM), Maud Kuistila
1051 Foundation (MM), Turku University Foundation (MM), Finnish Cancer Institute (TDL),
1052 Finnish Cultural Foundation (TDL), and Finnish Cultural Foundation (KJK).

1053 **References:**

- 1054 Adli M (2018) The CRISPR tool kit for genome editing and beyond. *Nat Commun* 9:
1055 1911
- 1056 Aguirre-Ghiso JA (2021) Translating the Science of Cancer Dormancy to the Clinic.
1057 *Cancer Res* 81: 4673-4675
- 1058 Arteaga CL, Engelman JA (2014) ERBB receptors: from oncogene discovery to
1059 basic science to mechanism-based cancer therapeutics. *Cancer Cell* 25: 282-303
- 1060 Berghoff AS, Bartsch R, Preusser M, Ricken G, Steger GG, Bago-Horvath Z, Rudas
1061 M, Streubel B, Dubsky P, Gnant M *et al* (2014) Co-overexpression of HER2/HER3 is
1062 a predictor of impaired survival in breast cancer patients. *Breast* 23: 637-643
- 1063 Berns K, Horlings HM, Hennessy BT, Madiredjo M, Hijmans EM, Beelen K, Linn SC,
1064 Gonzalez-Angulo AM, Stemke-Hale K, Hauptmann M *et al* (2007) A functional
1065 genetic approach identifies the PI3K pathway as a major determinant of trastuzumab
1066 resistance in breast cancer. *Cancer Cell* 12: 395-402
- 1067 [DATASET] Cerami E, Gao J, Dogrusoz U, Gross BE, Sumer SO, Aksoy BA,
1068 Jacobsen A, Byrne CJ, Heuer ML, Larsson E *et al* (2012) The cBio cancer genomics
1069 portal: an open platform for exploring multidimensional cancer genomics data.
1070 *Cancer Discov* 2: 401-404
- 1071 Chakraborty D, Kurppa KJ, Paatero I, Ojala VK, Koivu M, Tamirat MZ, Koivunen JP,
1072 Janne PA, Johnson MS, Elo LL *et al* (2019) An unbiased in vitro screen for activating
1073 epidermal growth factor receptor mutations. *J Biol Chem* 294: 9377-9389

1074 Chan LN, Murakami MA, Robinson ME, Caeser R, Sadras T, Lee J, Cosgun KN,
1075 Kume K, Khairnar V, Xiao G *et al* (2020) Signalling input from divergent pathways
1076 subverts B cell transformation. *Nature* 583: 845-851

1077 Chandarlapaty S, Sawai A, Scaltriti M, Rodrik-Outmezguine V, Grbovic-Huezo O,
1078 Serra V, Majumder PK, Baselga J, Rosen N (2011) AKT inhibition relieves feedback
1079 suppression of receptor tyrosine kinase expression and activity. *Cancer Cell* 19: 58-
1080 71

1081 [DATASET] Chang CA, Jen J, Jiang S, Sayad A, Mer AS, Brown KR, Nixon AML,
1082 Dhabaria A, Tang KH, Venet D *et al* (2022) Ontogeny and Vulnerabilities of Drug-
1083 Tolerant Persisters in HER2+ Breast Cancer. *Cancer discovery* 12: 1022-1045.
1084 <https://www.ncbi.nlm.nih.gov/geo/query/acc.cgi?acc=GSE155342>

1085 Cleary JM, McRee AJ, Shapiro GI, Tolaney SM, O'Neil BH, Kearns JD, Mathews S,
1086 Nering R, MacBeath G, Czibere A *et al* (2017) A phase 1 study combining the HER3
1087 antibody seribantumab (MM-121) and cetuximab with and without irinotecan. *Invest*
1088 *New Drugs* 35: 68-78

1089 Da Silva L, Simpson PT, Smart CE, Cocciardi S, Waddell N, Lane A, Morrison BJ,
1090 Vargas AC, Healey S, Beesley J *et al* (2010) HER3 and downstream pathways are
1091 involved in colonization of brain metastases from breast cancer. *Breast Cancer Res*
1092 12: R46

1093 [DATASET] de Bruijn I, Kundra R, Mastrogiacomo B, Tran TN, Sikina L, Mazor T, Li
1094 X, Ochoa A, Zhao G, Lai B *et al* (2023) Analysis and Visualization of Longitudinal
1095 Genomic and Clinical Data from the AACR Project GENIE Biopharma Collaborative
1096 in cBioPortal. *Cancer Res* 83: 3861-3867

1097 De Conti G, Dias MH, Bernards R (2021) Fighting Drug Resistance through the
1098 Targeting of Drug-Tolerant Persister Cells. *Cancers (Basel)* 13

- 1099 Dhimolea E, de Matos Simoes R, Kansara D, Al'Khafaji A, Bouyssou J, Weng X,
1100 Sharma S, Raja J, Awate P, Shirasaki R *et al* (2021) An Embryonic Diapause-like
1101 Adaptation with Suppressed Myc Activity Enables Tumor Treatment Persistence.
1102 *Cancer Cell* 39: 240-256 e211
1103 Erjala K, Sundvall M, Junntila TT, Zhang N, Savisalo M, Mali P, Kulmala J, Pulkkinen
1104 J, Grenman R, Elenius K (2006) Signaling via ErbB2 and ErbB3 associates with
1105 resistance and epidermal growth factor receptor (EGFR) amplification with sensitivity
1106 to EGFR inhibitor gefitinib in head and neck squamous cell carcinoma cells. *Clin*
1107 *Cancer Res* 12: 4103-4111
1108 Fecci PE, Champion CD, Hoj J, McKernan CM, Goodwin CR, Kirkpatrick JP, Anders
1109 CK, Pendergast AM, Sampson JH (2019) The Evolving Modern Management of
1110 Brain Metastasis. *Clin Cancer Res* 25: 6570-6580
1111 Futschik ME, Carlisle B (2005) Noise-robust soft clustering of gene expression time-
1112 course data. *J Bioinform Comput Biol* 3: 965-988
1113 Gaborit N, Abdul-Hai A, Mancini M, Lindzen M, Lavi S, Leitner O, Mounier L,
1114 Chentouf M, Dunoyer S, Ghosh M *et al* (2015) Examination of HER3 targeting in
1115 cancer using monoclonal antibodies. *Proc Natl Acad Sci U S A* 112: 839-844
1116 [DATASET] Gao J, Aksoy BA, Dogrusoz U, Dresdner G, Gross B, Sumer SO, Sun Y,
1117 Jacobsen A, Sinha R, Larsson E *et al* (2013) Integrative analysis of complex cancer
1118 genomics and clinical profiles using the cBioPortal. *Sci Signal* 6: pl1
1119 Goutsouliak K, Veeraraghavan J, Sethunath V, De Angelis C, Osborne CK, Rimawi
1120 MF, Schiff R (2020) Towards personalized treatment for early stage HER2-positive
1121 breast cancer. *Nat Rev Clin Oncol* 17: 233-250
1122 Gu Z, Eils R, Schlesner M (2016) Complex heatmaps reveal patterns and
1123 correlations in multidimensional genomic data. *Bioinformatics* 32: 2847-2849

- 1124 Haikala HM, Janne PA (2021) Thirty Years of HER3: From Basic Biology to
1125 Therapeutic Interventions. *Clin Cancer Res*
- 1126 Hanzelmann S, Castelo R, Guinney J (2013) GSVA: gene set variation analysis for
1127 microarray and RNA-seq data. *BMC Bioinformatics* 14: 7
- 1128 Hata AN, Niederst MJ, Archibald HL, Gomez-Caraballo M, Siddiqui FM, Mulvey HE,
1129 Maruvka YE, Ji F, Bhang HE, Krishnamurthy Radhakrishna V *et al* (2016) Tumor
1130 cells can follow distinct evolutionary paths to become resistant to epidermal growth
1131 factor receptor inhibition. *Nat Med* 22: 262-269
- 1132 Hudis C, Swanton C, Janjigian YY, Lee R, Sutherland S, Lehman R, Chandarlapaty
1133 S, Hamilton N, Gajria D, Knowles J *et al* (2013) A phase 1 study evaluating the
1134 combination of an allosteric AKT inhibitor (MK-2206) and trastuzumab in patients
1135 with HER2-positive solid tumors. *Breast Cancer Res* 15: R110
- 1136 Ianevski A, He L, Aittokallio T, Tang J (2017) SynergyFinder: a web application for
1137 analyzing drug combination dose-response matrix data. *Bioinformatics* 33: 2413-
1138 2415
- 1139 Kaltenmeier CT, Vollmer LL, Vernetti LA, Caprio L, Davis K, Korotchenko VN, Day
1140 BW, Tsang M, Hulkower KI, Lotze MT *et al* (2017) A Tumor Cell-Selective Inhibitor of
1141 Mitogen-Activated Protein Kinase Phosphatases Sensitizes Breast Cancer Cells to
1142 Lymphokine-Activated Killer Cell Activity. *J Pharmacol Exp Ther* 361: 39-50
- 1143 Keenan AB, Torre D, Lachmann A, Leong AK, Wojciechowicz ML, Utti V, Jagodnik
1144 KM, Kropiwnicki E, Wang Z, Ma'ayan A (2019) ChEA3: transcription factor
1145 enrichment analysis by orthogonal omics integration. *Nucleic Acids Res* 47: W212-
1146 W224
- 1147 Kesarwani M, Kincaid Z, Gomaa A, Huber E, Rohrbaugh S, Siddiqui Z, Bouso MF,
1148 Latif T, Xu M, Komurov K *et al* (2017) Targeting c-FOS and DUSP1 abrogates

1149 intrinsic resistance to tyrosine-kinase inhibitor therapy in BCR-ABL-induced
1150 leukemia. *Nat Med* 23: 472-482

1151 Knuefermann C, Lu Y, Liu B, Jin W, Liang K, Wu L, Schmidt M, Mills GB,
1152 Mendelsohn J, Fan Z (2003) HER2/PI-3K/Akt activation leads to a multidrug
1153 resistance in human breast adenocarcinoma cells. *Oncogene* 22: 3205-3212

1154 Kodack DP, Askokylakis V, Ferraro GB, Sheng Q, Badeaux M, Goel S, Qi X,
1155 Shankaraiah R, Cao ZA, Ramjiawan RR *et al* (2017) The brain microenvironment
1156 mediates resistance in luminal breast cancer to PI3K inhibition through HER3
1157 activation. *Sci Transl Med* 9

1158 Koivu MKA, Chakroborty D, Tamirat MZ, Johnson MS, Kurppa KJ, Elenius K (2021)
1159 Identification of Predictive ERBB Mutations by Leveraging Publicly Available Cell
1160 Line Databases. *Mol Cancer Ther* 20: 564-576

1161 Kong T, Laranjeira ABA, Yang K, Fisher DAC, Yu L, Poittevin De La Fregonnier L,
1162 Wang AZ, Ruzinova MB, Fowles JS, Fulbright MC *et al* (2023) DUSP6 mediates
1163 resistance to JAK2 inhibition and drives leukemic progression. *Nat Cancer* 4: 108-
1164 127

1165 Korotchenko VN, Saydmohammed M, Vollmer LL, Bakan A, Sheetz K, Debiec KT,
1166 Greene KA, Agliori CS, Bahar I, Day BW *et al* (2014) In vivo structure-activity
1167 relationship studies support allosteric targeting of a dual specificity phosphatase.
1168 *Chembiochem* 15: 1436-1445

1169 Kurppa KJ, Liu Y, To C, Zhang T, Fan M, Vajdi A, Knelson EH, Xie Y, Lim K, Cejas P
1170 *et al* (2020) Treatment-Induced Tumor Dormancy through YAP-Mediated
1171 Transcriptional Reprogramming of the Apoptotic Pathway. *Cancer Cell* 37: 104-122
1172 e112

1173 Lazo JS, McQueeney KE, Burnett JC, Wipf P, Sharlow ER (2018) Small molecule
1174 targeting of PTPs in cancer. *Int J Biochem Cell Biol* 96: 171-181

1175 Leung WY, Roxanis I, Sheldon H, Buffa FM, Li JL, Harris AL, Kong A (2015)
1176 Combining lapatinib and pertuzumab to overcome lapatinib resistance due to NRG1-
1177 mediated signalling in HER2-amplified breast cancer. *Oncotarget* 6: 5678-5694

1178 Majewski IJ, Nuciforo P, Mittempergher L, Bosma AJ, Eidtmann H, Holmes E,
1179 Sotiriou C, Fumagalli D, Jimenez J, Aura C *et al* (2015) PIK3CA mutations are
1180 associated with decreased benefit to neoadjuvant human epidermal growth factor
1181 receptor 2-targeted therapies in breast cancer. *J Clin Oncol* 33: 1334-1339

1182 Marine JC, Dawson SJ, Dawson MA (2020) Non-genetic mechanisms of therapeutic
1183 resistance in cancer. *Nat Rev Cancer* 20: 743-756

1184 Marsolier J, Prompsy P, Durand A, Lyne AM, Landragin C, Trouchet A, Bento ST,
1185 Eisele A, Foulon S, Baudre L *et al* (2022) H3K27me3 conditions chemotolerance in
1186 triple-negative breast cancer. *Nat Genet* 54: 459-468

1187 Merisaari J, Denisova OV, Doroszko M, Le Joncour V, Johansson P, Leenders WPJ,
1188 Kastrinsky DB, Zaware N, Narla G, Laakkonen P *et al* (2020) Monotherapy efficacy
1189 of blood-brain barrier permeable small molecule reactivators of protein phosphatase
1190 2A in glioblastoma. *Brain Commun* 2: fcaa002

1191 Molina G, Vogt A, Bakan A, Dai W, Queiroz de Oliveira P, Znosko W, Smithgall TE,
1192 Bahar I, Lazo JS, Day BW *et al* (2009) Zebrafish chemical screening reveals an
1193 inhibitor of Dusp6 that expands cardiac cell lineages. *Nat Chem Biol* 5: 680-687

1194 Murthy RK, Loi S, Okines A, Paplomata E, Hamilton E, Hurvitz SA, Lin NU, Borges
1195 V, Abramson V, Anders C *et al* (2020) Tucatinib, Trastuzumab, and Capecitabine for
1196 HER2-Positive Metastatic Breast Cancer. *N Engl J Med* 382: 597-609

- 1197 Nagata Y, Lan KH, Zhou X, Tan M, Esteva FJ, Sahin AA, Klos KS, Li P, Monia BP,
1198 Nguyen NT *et al* (2004) PTEN activation contributes to tumor inhibition by
1199 trastuzumab, and loss of PTEN predicts trastuzumab resistance in patients. *Cancer*
1200 *Cell* 6: 117-127
- 1201 Nichols A, Camps M, Gillieron C, Chabert C, Brunet A, Wilsbacher J, Cobb M,
1202 Pouyssegur J, Shaw JP, Arkinstall S (2000) Substrate recognition domains within
1203 extracellular signal-regulated kinase mediate binding and catalytic activation of
1204 mitogen-activated protein kinase phosphatase-3. *J Biol Chem* 275: 24613-24621
- 1205 Patterson KI, Brummer T, O'Brien PM, Daly RJ (2009) Dual-specificity
1206 phosphatases: critical regulators with diverse cellular targets. *Biochem J* 418: 475-
1207 489
- 1208 Pereira B, Chin SF, Rueda OM, Volland HK, Provenzano E, Bardwell HA, Pugh M,
1209 Jones L, Russell R, Sammut SJ *et al* (2016) The somatic mutation profiles of 2,433
1210 breast cancers refines their genomic and transcriptomic landscapes. *Nature*
1211 *communications* 7: 11479
- 1212 Ramkissoon A, Chaney KE, Milewski D, Williams KB, Williams RL, Choi K, Miller A,
1213 Kalin TV, Pressey JG, Szabo S *et al* (2019) Targeted Inhibition of the Dual
1214 Specificity Phosphatases DUSP1 and DUSP6 Suppress MPNST Growth via JNK.
1215 *Clin Cancer Res* 25: 4117-4127
- 1216 Recondo G, Bahcall M, Spurr LF, Che J, Ricciuti B, Leonardi GC, Lo YC, Li YY,
1217 Lamberti G, Nguyen T *et al* (2020) Molecular Mechanisms of Acquired Resistance to
1218 MET Tyrosine Kinase Inhibitors in Patients with MET Exon 14-Mutant NSCLC. *Clin*
1219 *Cancer Res* 26: 2615-2625

- 1220 Ritchie ME, Phipson B, Wu D, Hu Y, Law CW, Shi W, Smyth GK (2015) limma
1221 powers differential expression analyses for RNA-sequencing and microarray studies.
1222 *Nucleic Acids Res* 43: e47
- 1223 Saddoughi SA, Gencer S, Peterson YK, Ward KE, Mukhopadhyay A, Oaks J,
1224 Bielawski J, Szulc ZM, Thomas RJ, Selvam SP et al (2013) Sphingosine analogue
1225 drug FTY720 targets I2PP2A/SET and mediates lung tumour suppression via
1226 activation of PP2A-RIPK1-dependent necroptosis. *EMBO Mol Med* 5: 105-121
- 1227 Saura C, Bendell J, Jerusalem G, Su S, Ru Q, De Buck S, Mills D, Ruquet S, Bosch
1228 A, Urruticoechea A et al (2014) Phase Ib study of Buparlisib plus Trastuzumab in
1229 patients with HER2-positive advanced or metastatic breast cancer that has
1230 progressed on Trastuzumab-based therapy. *Clin Cancer Res* 20: 1935-1945
- 1231 Saura C, Oliveira M, Feng YH, Dai MS, Chen SW, Hurvitz SA, Kim SB, Moy B,
1232 Delaloge S, Gradishar W et al (2020) Neratinib Plus Capecitabine Versus Lapatinib
1233 Plus Capecitabine in HER2-Positive Metastatic Breast Cancer Previously Treated
1234 With 2 HER2-Directed Regimens: Phase III NALA Trial. *J Clin Oncol* 38: 3138-3149
- 1235 Schneeweiss A, Park-Simon TW, Albanell J, Lassen U, Cortes J, Dieras V, May M,
1236 Schindler C, Marme F, Cejalvo JM et al (2018) Phase Ib study evaluating safety and
1237 clinical activity of the anti-HER3 antibody lumretuzumab combined with the anti-
1238 HER2 antibody pertuzumab and paclitaxel in HER3-positive, HER2-low metastatic
1239 breast cancer. *Invest New Drugs* 36: 848-859
- 1240 Sharma SV, Lee DY, Li B, Quinlan MP, Takahashi F, Maheswaran S, McDermott U,
1241 Azizian N, Zou L, Fischbach MA et al (2010) A chromatin-mediated reversible drug-
1242 tolerant state in cancer cell subpopulations. *Cell* 141: 69-80
- 1243 Shojaee S, Caeser R, Buchner M, Park E, Swaminathan S, Hurtz C, Geng H, Chan
1244 LN, Klemm L, Hofmann WK et al (2015) Erk Negative Feedback Control Enables

1245 Pre-B Cell Transformation and Represents a Therapeutic Target in Acute
1246 Lymphoblastic Leukemia. *Cancer Cell* 28: 114-128

1247 Thompson EM, Patel V, Rajeeve V, Cutillas PR, Stoker AW (2022) The cytotoxic
1248 action of BCI is not dependent on its stated DUSP1 or DUSP6 targets in
1249 neuroblastoma cells. *FEBS Open Bio* 12: 1388-1405

1250 Vainonen JP, Momeny M, Westermarck J (2021) Druggable cancer phosphatases.
1251 *Sci Transl Med* 13

1252 Wang SP, Wu SQ, Huang SH, Tang YX, Meng LQ, Liu F, Zhu QH, Xu YG (2021)
1253 FDI-6 inhibits the expression and function of FOXM1 to sensitize BRCA-proficient
1254 triple-negative breast cancer cells to Olaparib by regulating cell cycle progression
1255 and DNA damage repair. *Cell death & disease* 12: 1138

1256 Wilson TR, Fridlyand J, Yan Y, Penuel E, Burton L, Chan E, Peng J, Lin E, Wang Y,
1257 Sosman J *et al* (2012) Widespread potential for growth-factor-driven resistance to
1258 anticancer kinase inhibitors. *Nature* 487: 505-509

1259 Wu QN, Liao YF, Lu YX, Wang Y, Lu JH, Zeng ZL, Huang QT, Sheng H, Yun JP, Xie
1260 D *et al* (2018) Pharmacological inhibition of DUSP6 suppresses gastric cancer
1261 growth and metastasis and overcomes cisplatin resistance. *Cancer Lett* 412: 243-
1262 255

1263 Xie T, Lim SM, Westover KD, Dodge ME, Ercan D, Ficarro SB, Udayakumar D,
1264 Gurbani D, Tae HS, Riddle SM *et al* (2014) Pharmacological targeting of the
1265 pseudokinase Her3. *Nat Chem Biol* 10: 1006-1012

1266 Yonesaka K, Zejnullahu K, Okamoto I, Satoh T, Cappuzzo F, Souglakos J, Ercan D,
1267 Rogers A, Roncalli M, Takeda M *et al* (2011) Activation of ERBB2 signaling causes
1268 resistance to the EGFR-directed therapeutic antibody cetuximab. *Sci Transl Med* 3:
1269 99ra86

- 1270 Zandi Z, Kashani B, Alishahi Z, Pourbagheri-Sigaroodi A, Esmaeili F, Ghaffari SH,
1271 Bashash D, Momeny M (2022) Dual-specificity phosphatases: therapeutic targets in
1272 cancer therapy resistance. *J Cancer Res Clin Oncol* 148: 57-70
- 1273 Zhang S, Huang WC, Zhang L, Zhang C, Lowery FJ, Ding Z, Guo H, Wang H,
1274 Huang S, Sahin AA *et al* (2013) SRC family kinases as novel therapeutic targets to
1275 treat breast cancer brain metastases. *Cancer Res* 73: 5764-5774
- 1276 Zhang YL, Ma Y, Zeng YQ, Liu Y, He EP, Liu YT, Qiao FL, Yu R, Wang YS, Wu XY
1277 *et al* (2021) A narrative review of research progress on FoxM1 in breast cancer
1278 carcinogenesis and therapeutics. *Ann Transl Med* 9: 1704
- 1279 Zheng R, Wan C, Mei S, Qin Q, Wu Q, Sun H, Chen CH, Brown M, Zhang X, Meyer
1280 CA *et al* (2019) Cistrome Data Browser: expanded datasets and new tools for gene
1281 regulatory analysis. *Nucleic Acids Res* 47: D729-D735
- 1282
- 1283
- 1284
- 1285

1286

1287 **Figure legends**

1288

1289 **Figure 1: Transcriptional landscape of lapatinib tolerance and resistance**

1290 **development in HER2+ cells.** **(A)** Development of lapatinib resistance in HER2+

1291 breast cancer cells. BT474 and BT474Br cells were treated with 1 μ M of lapatinib for

1292 9 days (d), 6 months (mos) and 9 mos to yield Drug-tolerant persister (DTP), Drug-

1293 tolerant expanding perister (DTEP) and Long term resistant (LR) clones,

1294 respectively. The cells were stained with crystal violet (0.5% w/v) and the images

1295 were acquired with an inverted microscope. The transcriptional profiles from each

1296 functional state of lapatinib drug tolerance and resistance development from three

1297 parallel BT474 cell plates were surveyed by RNA-sequencing. **(B)** The number of the

1298 genes with a significant change in their expression during the resistance acquisition

1299 (see Dataset EV1 for individual gene names). Transcription factor (TF) binding motifs

1300 significantly enriched in significantly regulated genes in each transition are indicated.

1301 Bolding indicates shared TF binding sites between DTP downregulated and DTEP

1302 upregulated genes. **(C)** Differentially expressed pathways were identified using the R

1303 package limma and hallmark gene sets were used for GSVA analysis to reveal

1304 hallmarks and signal transduction pathways involved in each step of the resistance

1305 acquisition. Red indicates those hallmarks and pathways that are overlapping with

1306 processes regulated by DUSP6 depletion in figure 3F.

1307

1308 **Figure 2: Clinical association of *DUSP6* overexpression with poor prognosis**

1309 **HER2+ breast cancers.** **(A, B)** Volcano plots visualizing differentially expressed

1310 genes in (A) Control-DTP and (B) DTP-DTEP transitions. The volcano blots indicate

1311 all genes that were significantly regulated during these transitions ($|logFC| < 2$ and
1312 FDR < 0.05), whereas only the phosphatase genes among these are indicated by
1313 names. The four phosphatase genes significantly regulated in both transitions
1314 (*DUSP6*, *CDC25A*, *CDC25C*, and *SYNJ1*) are indicated in bold. Differentially
1315 expressed genes were identified using the R package limma (n=3). **(C)** Changes in
1316 the *DUSP6*, *CDC25A*, *CDC25C*, and *SYNJ1* mRNA levels during the acquisition of
1317 lapatinib resistance in BT474 cells. Data is based on RNA sequencing analysis
1318 (Dataset EV1) and was analyzed by one-way ANOVA followed by Tukey's multiple
1319 comparisons test. Statistically significant values of * $p < 0.05$, ** $p < 0.01$ and *** $p <$
1320 0.001 were determined (n=3). **(D)** Differential expression of *DUSP6*, *CDC25A*,
1321 *CDC25C*, and *SYNJ1* in different breast cancer subtypes. Data were extracted from
1322 the METABRIC dataset and categorized into five molecular subtypes according to
1323 the PAM50 gene expression subtype classification (basal, claudin-low, HER2+,
1324 Luminal A, and Luminal B). Data were analyzed by one-way ANOVA followed by
1325 Tukey's multiple comparisons test and shown as mean \pm standard deviation (SD).
1326 Statistically significant values of * $p < 0.05$, ** $p < 0.01$ and **** $p < 0.0001$ were
1327 determined (basal=209, claudin-low=218, HER2+=224, LumA=700 and LumB=475).
1328 **(E)** Breast cancer patients from the TCGA-BRCA dataset were divided into *DUSP6*
1329 high ($LogFC > 1$, FDR < 0.05) and low expression ($LogFC < -1$, FDR < 0.05) groups and
1330 the clinical breast cancer subtypes were compared between the two groups. NA; not
1331 available. **(F,G)** Subgroup of 113 patient cases with high tumor *ERBB2* mRNA
1332 expression ($LogFC > 1$, FDR < 0.05) were divided into *DUSP6*high and *DUSP6*low
1333 groups and their overall survival (OS) (G) (Log-rank Test p value=0.0220) and
1334 disease-specific progression free survival (PFS)(H)(Log-rank Test p value=0.0259)
1335 was tested according to *DUSP6* status.

1336

1337 **Figure 3: Functional involvement of DUSP6 in HER2i tolerance development.**

1338 **(A)** Expression of DUSP6 protein in different stages of lapatinib resistance
1339 development by Western blot analysis. **(B)** Relative expression of *DUSP6* mRNA in
1340 indicated cell lines either at the untreated control situation, or in the DTP state after
1341 following treatments: BT474Br, Lapatinib 1 μ M for 9 days; EFM192A and HCC1419,
1342 Lapatinib 2.5 μ M for 14 days; HCC827(EGFRmut NSCLC), 1 μ M Osimertinib for 10
1343 days; A375(BRAFV600E mutant malignant melanoma (MM)), 1 μ M dabrafenib+100
1344 nM trametinib for 10 days; and HT-29(BRAFV600E mutant colorectal cancer (CRC)),
1345 1 μ M dabrafenib+10 μ g/ml cetuximab for 10 days. Data for EFM192 and HCC1419
1346 cells was obtained from (DataRef: (Chang *et al.*, 2022)(GSE155342), and for other
1347 cells by qRT-PCR analysis of the *de novo* treated samples. Shown is data from two-
1348 three repeat samples. **(C)** Transcriptional profile of MDA-MB-453 cells after *DUSP6*
1349 knockdown by 3 different siRNA and compared with 3 different scramble controls,
1350 followed by the GSVA analysis of the Hallmark gene sets. The Hallmark gene sets
1351 overlapping with the gene sets regulated to same direction in DUSP6 low expressing
1352 DTEP cells (Fig. 1C) are indicated with red. **(D, E)** Ectopic overexpression of
1353 DUSP6 in BT474 cells inhibits lapatinib effects on cell viability (G) and apoptosis (H),
1354 as measured by WST1 cell viability assay and caspase 3/7 activity, respectively.
1355 Data was analyzed by two-way ANOVA followed by Tukey' post hoc test.
1356 Statistically significant values of ** $p < 0.01$ and **** $p < 0.0001$ were determined. n=3.
1357 **(F)** Ectopic overexpression of either wild-type DUSP6 (DUSPWT) or ERK binding
1358 deficient KIM mutant of DUSP6 (DUSP6MUT) in BT474 cells inhibits lapatinib effects
1359 on apoptosis. Shown is a result from a representative experiment from three repeats
1360 with similar results. Data were analyzed by two-way ANOVA followed by Tukey' post

1361 hoc test. Statistically significant values of $**p < 0.01$ and $****p < 0.0001$ were
1362 determined. **(G)** DUSP6 inhibitor BCI preempts DTEP development in BT474 cells
1363 treated with either lapatinib or neratinib for 6 months. The cells were stained and
1364 fixed with crystal violet in methanol (0.5% w/v) and the images were acquired with an
1365 inverted microscope.

1366

1367 **Figure 4: Both genetic and pharmacological DUSP6 targeting overcomes**
1368 **HER2i resistance.** **(A)** RNAi-mediated *DUSP6* knockdown, but not of *DUSP1*,
1369 induces apoptotic cell death in MDA-MB-453 cells, as shown by Western blotting for
1370 PARP-1 cleavage. **(B)** CRISPR/CAS9-mediated *DUSP6* knockout hinders the
1371 clonogenic growth of MDA-MB-453 cells, as compared to the CAS9 expressing
1372 controls. Shown are three independent single cell clones created with two
1373 independent gRNAs (g1 and g2). The cells were seeded at low density and
1374 maintained for 10 d. The colonies were stained/fixed with 0.5% crystal violet in
1375 methanol and imaged using an inverted microscope. **(C)** *DUSP6* siRNA knockdown
1376 increases sensitivity of HER2i resistant MDA-MB-453 cells to HER2-targeted
1377 therapies. Cell viability was measured by WST-1 assay after 48 h of drug treatment.
1378 Data were collected from three independent experiments each performed in triplicate
1379 and analyzed by one-way ANOVA followed by Tukey's multiple comparisons test.
1380 Statistically significant values of $**p < 0.01$, $***p < 0.001$ and $****p < 0.0001$ were
1381 determined. **(D)** A 2D synergy map of neratinib-BCI combination in MDA-MB-453
1382 cells calculated by Bliss SynergyFinder (lanevski *et al.*, 2017). Higher score (in red)
1383 indicates for higher degree of drug synergy. The cultures were treated with
1384 increasing concentrations of the compounds for 48 h and cell viability was measured
1385 by WST-1 assay. **(E)** *DUSP6* siRNA knockdown increases sensitivity of HER2i

1386 resistant MDA-MB-453 cells to combination with capecitabine and neratinib. Cell
1387 viability was measured by WST-1 assay after 48 h of drug treatment. Data were
1388 collected from three independent experiments each performed in triplicate and
1389 analyzed by one-way ANOVA followed by Tukey's multiple comparisons test.
1390 Statistically significant values of *** $p < 0.0001$ were determined.

1391

1392 **Figure 5: DUSP6 inhibition overcomes HER2 inhibitor resistance *in vivo*. (A)**
1393 Subcutaneous xenograft growth of two independent *DUSP6* single cell knockout
1394 clones of MDA-MB-453 cells targeted with two different gRNA guides. One-way
1395 ANOVA followed by Tukey's multiple comparisons test ** $p < 0.01$ comparing each
1396 clone to CAS9 expressing control cells . Data are shown as mean \pm SD (n=5) **(B-E)**
1397 The effect of BCI in combination with lapatinib or neratinib in two HER2 inhibitor
1398 resistant xenograft models: HCC1954 **(B, C)** or MDA-MB-453 **(D, E)**. Data are shown
1399 as mean \pm SD (n=10 in each treatment group). Mice with tumor size \sim 100 mm³ were
1400 randomized into the experimental and the control groups and tumor volumes were
1401 measured every 3 d. Data were analyzed by one-way ANOVA followed by Tukey's
1402 multiple comparisons test. Statistically significant values of *** $p < 0.0001$ were
1403 determined. **C** and **E** panels display percentual change in the tumor volume from the
1404 start of the therapy as water-fall blots in HCC1954 and MDA-MB453 models,
1405 respectively. **(F)** H&E staining of the representative MDA-MB-453 xenograft tumors
1406 from the control, lapatinib, BCI and lapatinib+BCI groups at day 24. Scale bar 200
1407 μ m.

1408

1409 **Figure 6: DUSP6 targeting inhibits HER3 expression (A)** A 2D synergy map of
1410 lapatinib+MK2206(AKTi) or **(B)** lapatinib+BCI(DUSP6i) combination in MDA-MB-453

1411 cells calculated by the Bliss SynergyFinder. Higher score (in red) indicates for higher
1412 degree of drug synergy. The cultures were treated with increasing concentrations of
1413 the compounds for 48 h and cell viability was measured by WST-1 assay. **(C)**
1414 Comparison of the effects of lapatinib+BCI and lapatinib+MK2206 on apoptosis
1415 induction (PARP-1 cleavage), and HER2 or HER3 protein levels by Western blot
1416 analysis. The cells were treated with lapatinib (1 μ M), MK2206 (2.5 μ M) and BCI (2.5
1417 μ M) and their combinations for 48 h. **(D)** Quantification of PARP1 cleavage from
1418 three repeats of (C). Data were analyzed by one-way ANOVA followed by Tukey's
1419 multiple comparisons test. Statistically significant values of ** $p < 0.01$ and **** $p <$
1420 0.0001 were determined. **(E,F)** The dose-dependent effects of MK2206 (E) and BCI
1421 (F) on the expression of HER2 and HER3 protein levels in MDA-MB-453 cells by
1422 Western blot analysis after 48h of treatment. **(G)** The time-dependent effects of BCI
1423 (2.5 μ M) on the expression of HER2 and HER3 protein levels and apoptosis
1424 induction (PARP cleavage) in MDA-MB-453 cells by Western blot analysis. Increase
1425 in phosphorylated ERK (p-ERK1/2) and inhibition of DUSP6 both indicate for early
1426 target engagement by BCI. **(H)** DUSP6 knockdown by siRNA inhibits HER2 and
1427 HER3 protein expression in MDA-MB-453 cells. **(I)** Effects of BCI (50 mg/kg) therapy
1428 on HER2 and HER3 protein levels in the MDA-MB-453 xenograft tissue on day 24.
1429 Shown is immunohistochemical analysis of HER2 and HER3 from the adjacent
1430 paraffin embedded tissue slices from Fig. 5F. Scale bar 200 μ m. **(J)** Breast cancer
1431 patients from the TCGA-BRCA dataset were divided into DUSP6 high ($\text{LogFC} > 1$,
1432 $\text{FDR} < 0.05$) and low expression ($\text{LogFC} < -1$, $\text{FDR} < 0.05$) profiles and expression of
1433 phosphorylated HER3 ($\text{p-HER3}^{\text{Y}1298}$) was compared between the two groups. Data
1434 were analyzed by two-tailed t test; ** $p < 0.01$. (DUSP6high=142, DUSP6low=149).
1435

1436 **Fig. 7. DUSP6 targeting overcomes Neuregulin/HER3-mediated HER2i therapy**
1437 **tolerance**

1438 **(A)** Comparison of the potential of BCI or MK2206 treatment to overcome Neuregulin
1439 (NRG)-mediated rescue from the anti-proliferative activity of neratinib. The cells were
1440 treated with NRG (10 ng/mL), lapatinib (1 μ M), MK2206 (1, 2.5, and 5 μ M), and BCI
1441 (1, 2.5, and 5 μ M) for 48 h and cell viability was measured by WST-1 assay. Data
1442 were collected from three independent experiments each performed with three
1443 technical repeat samples. **(B)** Comparison of the effects of BCI and MK2206 on
1444 NRG-mediated evasion from neratinib-induced apoptotic cell death, as measured by
1445 Western blot analysis for cleaved PARP-1. The cells were treated with NRG (10
1446 ng/mL), lapatinib (1 μ M), MK2206 (2.5 μ M) and BCI (2.5 μ M) for 48 h. **(C)** HER3
1447 overexpression rescues MDA-MB-453 cells from BCI-elicited inhibition of cell
1448 viability. The control or HER3 overexpressing MDA-MB-453 were treated with BCI (3
1449 μ M) for 48 h and cell viability was measured by WST-1 assay. Shown is data from
1450 four technical replicate samples from a representative of three experiments with
1451 similar results. The data was analysed by Two-way ANOVA + Tukey's post hoc test,
1452 **** $p < 0.0001$ **(D)** Comparison of the effects of lapatinib+BCI and lapatinib+MK2206
1453 on NRG-mediated rescue from the anti-growth activity of lapatinib, as shown by
1454 crystal violet staining. The cells were treated with NRG (10 ng/mL), lapatinib (1 μ M),
1455 MK2206 (2.5 μ M) and BCI (2.5 μ M) for 48 h, stained/fixed with 0.5% crystal violet in
1456 methanol and imaged by an inverted microscope (images acquired at 10x
1457 magnification). **(E)** Breast cancer patients from the TCGA-BRCA dataset were
1458 divided into *DUSP6* high (LogFC>1, FDR<0.05) and low expression (LogFC<-1,
1459 FDR<0.05) profiles and the neuregulin (*NRG1*) mRNA levels were compared
1460 between the two groups. Data were analyzed by two-tailed t test; **** $p < 0.0001$.

1461 (DUSP6high=167, DUSP6low=181). **(F)** The effect of *DUSP6* knockdown on the
1462 brain metastatic outgrowth of MDA-MB-361 cells in a zebrafish model. GFP positive
1463 MDA-MB-361 cells transfected either with control scrambled siRNA or DUSP6 siRNA
1464 were injected into zebrafish embryo brain and the GFP intensity was measured 3
1465 days after by microscopy. Data were analyzed by two-tailed *t* test; *****p* < 0.0001.
1466 Scale bar 100 μ m (siSCR=37, siDUSP6=43). **(G)** Improved overall survival of mice
1467 with intracranially injected DUSP6 KO MDA-MB-453 cells as compared to the CAS9
1468 positive control cell injected mice. Survival data were analyzed by log-rank Mantel–
1469 Cox test, ***p* < 0.01.

1470

1471 **Figure 8. Feed-forward loop between NRG/HER3 and DUSP6 determines HER2i
1472 sensitivity**

1473

1474 **(A)** *DUSP1* and *DUSP6* mRNA levels were determined by qRT-PCR analysis after
1475 treatment with increasing concentrations of neratinib for 48 h in indicated cell lines.
1476 Red denotes for HER2i resistant cell lines and green HER2i sensitive cells. Data
1477 were collected from three independent experiments each performed in triplicate. **(B,**
1478 **C)** Comparison of the effect of neratinib treatment (48 h) on DUSP6, p-AKT and p-
1479 ERK1/2 between HER2i sensitive BT474Br (B) and HER2i resistant MDA-MB-361
1480 (C) cells, respectively. **(D)** The effect of siRNA-mediated *HER3* knockdown on
1481 DUSP6 expression in MDA-MB-453 cells by Western blot analysis. **(E)** NRG-
1482 mediated induction of *DUSP6* mRNA via MEK activation as measured by qRT-PCR
1483 analysis after treatment with NRG (10 ng/mL), MK2206(AKTi) (2.5 μ M), and
1484 trametinib(MEKi) (100 nM) for 48 h. Data were analyzed by one-way ANOVA
1485 followed by Tukey's multiple comparisons test. Statistically significant values of **p* <

1486 0.05 and **** $p < 0.0001$ were determined (n=3). **(F)** The effect of NRG on DUSP6
1487 protein expression BT474 cells via MEK activation. The cells were serum-starved for
1488 24 h, followed by treatment with NRG (10 ng/mL), MK2206 (2.5 μ M) and trametinib
1489 (100 nM) for 48 h. **(G)** Inhibition of DUSP6 expression in HER2i resistant MDA-MB-
1490 453 cells by MEKi Trametinib. The cells were treated with MK2206 (2.5 μ M) or
1491 trametinib (100 nM) for 48 h. **(H)** A schematic illustration of the discovered
1492 HER3/DUSP6 feed forward loop in HER2+ breast cancer cells. NRG binding to
1493 HER3 induces MEK/ERK-mediated *DUSP6* expression which feeds back to
1494 increased HER2 and HER3 expression (left panel). In HER2i sensitive cells (middle
1495 panel) inhibition of HER3 results in *DUSP6* inhibition and loss of DUSP6 driven
1496 cancer hallmarks. In HER2i resistant cells (right panel), MEK is not inhibited by
1497 HER2i but its constitutive activity (MEKca.) drives DUSP6-HER2/3 positive feed-
1498 back loop resulting in HER3-mediated multitherapy resistance and cancer
1499 progression.

1500

1501 **Expanded view figure legends**

1502

1503 **Figure EV1: Profiling of a panel of HER2+ breast cancer cell lines for their
1504 sensitivity to HER2 targeting small molecule tyrosine kinase inhibitors**

1505 The primary HER2i sensitive cells are marked on green, and the acquired HER2i
1506 resistant cells in red. The long-term resistant (LR) BT-474 and BT-474Br generated
1507 by 9-month treatment with lapatinib in this study are denoted in bold. The cells were
1508 treated with the increasing concentrations of the indicated HER2i compounds (in μ M)
1509 for 48 h and cell viability was measured using WST-1 assay.

1510

1511 **Figure EV2: E2F1 and FOXM1 target genes are inhibited across HER2+ DTP**
1512 **cells**

1513 **A)** mRNA levels of selected predicted FOXM1 and E2F1 target genes regulated
1514 during different steps of acquisition of lapatinib resistance in BT474 cells (Fig. 1).
1515 Data is blotted based on RNA sequencing analysis (Dataset EV1). **(B, C)** Expression
1516 of the predicted FOXM1 and E2F1 target genes in HER2+ HCC1419 and EFM192A
1517 cells between the DTP and the control cells. The RNA-seq data was obtained from
1518 (Dataref: (Chang *et al.*, 2022)(GSE155342). The cells were treated with lapatinib (2.5
1519 μ M) for 14 days to reach the DTP state. Data are shown as mean \pm SD (n=2) **(D)**
1520 Changes in the expression of FOXM1, PLK1, CCNB1, E2F1, CCNE2 and CDC6 in
1521 BT474Br cells between the control and the DTP cells treated for 9 days with lapatinib
1522 (1 μ M). Data is based on Q-PCR analysis from three technical replicates. The
1523 analysis was limited to only these genes due to lack of sufficient mRNA material from
1524 the strongly growth suppressed DTP cells. Data are shown as mean \pm SD (n=3).

1525

1526 **Figure EV3: DUSP6 overexpression protects HER2+ cells from HER2i-induced**
1527 **cell death**

1528 **(A, B)** Ectopic overexpression of DUSP6 in BT474 cells inhibits neratinib-elicited
1529 effects on cell viability and apoptosis, as measured by WST1 cell viability assay and
1530 caspase 3/7 activity, respectively. Data were collected from three independent
1531 experiments each performed in triplicate and analyzed by two-way ANOVA followed
1532 by Tukey' post hoc test. Statistically significant values of **** $p < 0.0001$ were
1533 determined. **(C)** Ectopic overexpression of DUSP6 in BT474 cells inhibits the
1534 afatinib-elicited effects on cell viability, as measured by WST1 assay. Data were
1535 collected from three independent experiments each performed in triplicate and

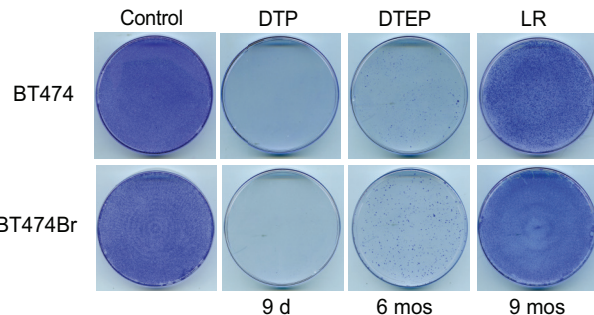
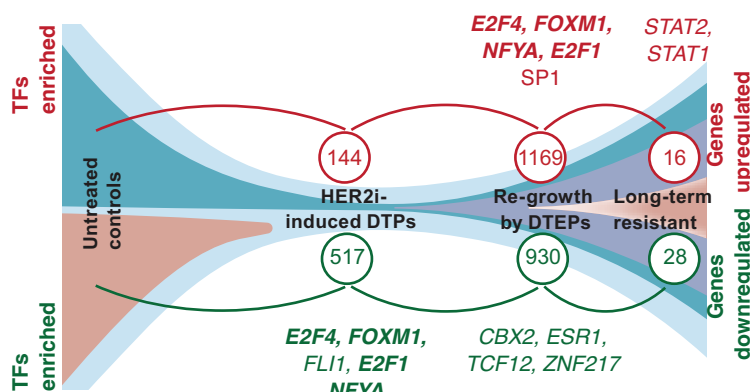
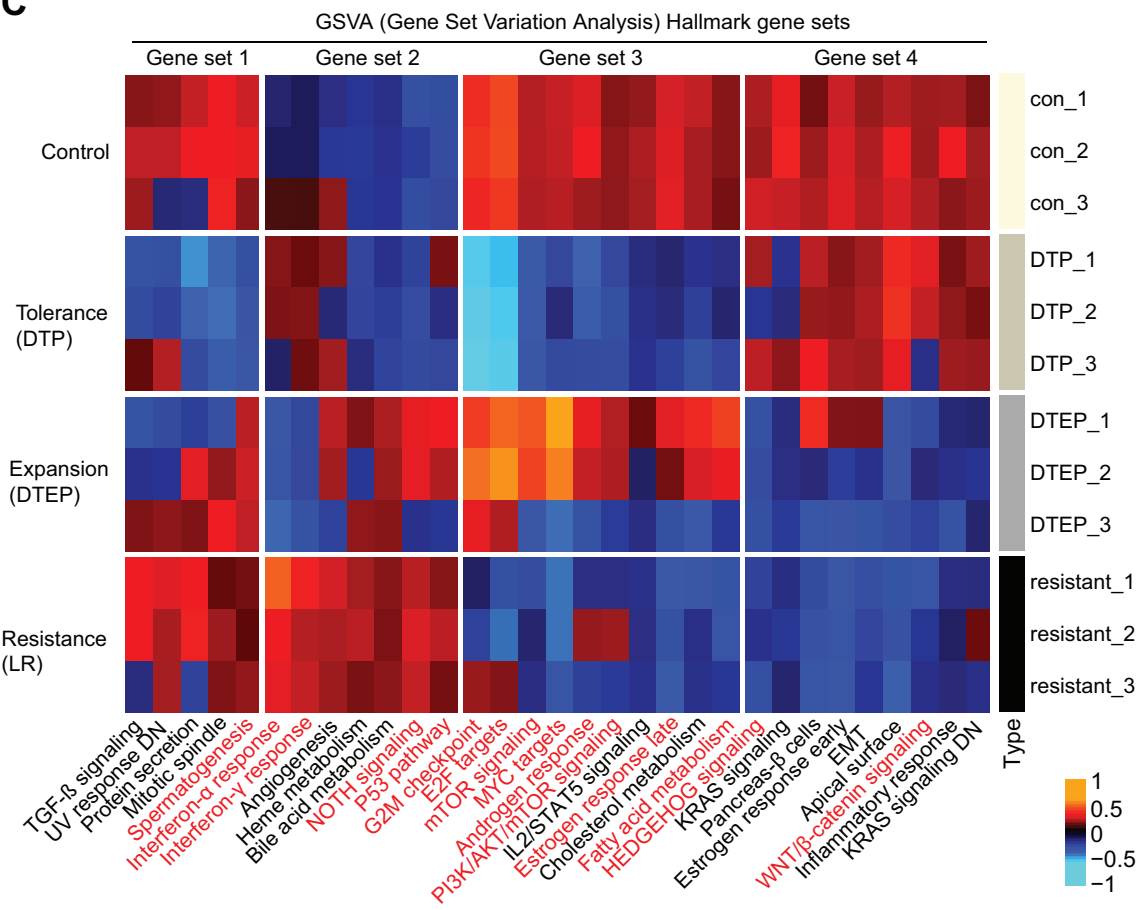
1536 analyzed by two-way ANOVA followed by Tukey' post hoc test. Statistically
1537 significant values of **** $p < 0.0001$ were determined. **(D)** Ectopic overexpression of
1538 DUSP6, but not of DUSP1, inhibits the Tucatinib-elicited effects on cell viability, as
1539 measured by WST1 assay. Data were collected from three independent experiments
1540 each performed in triplicate and analyzed by two-way ANOVA followed by Tukey'
1541 post hoc test. Statistically significant values of **** $p < 0.0001$ were determined.

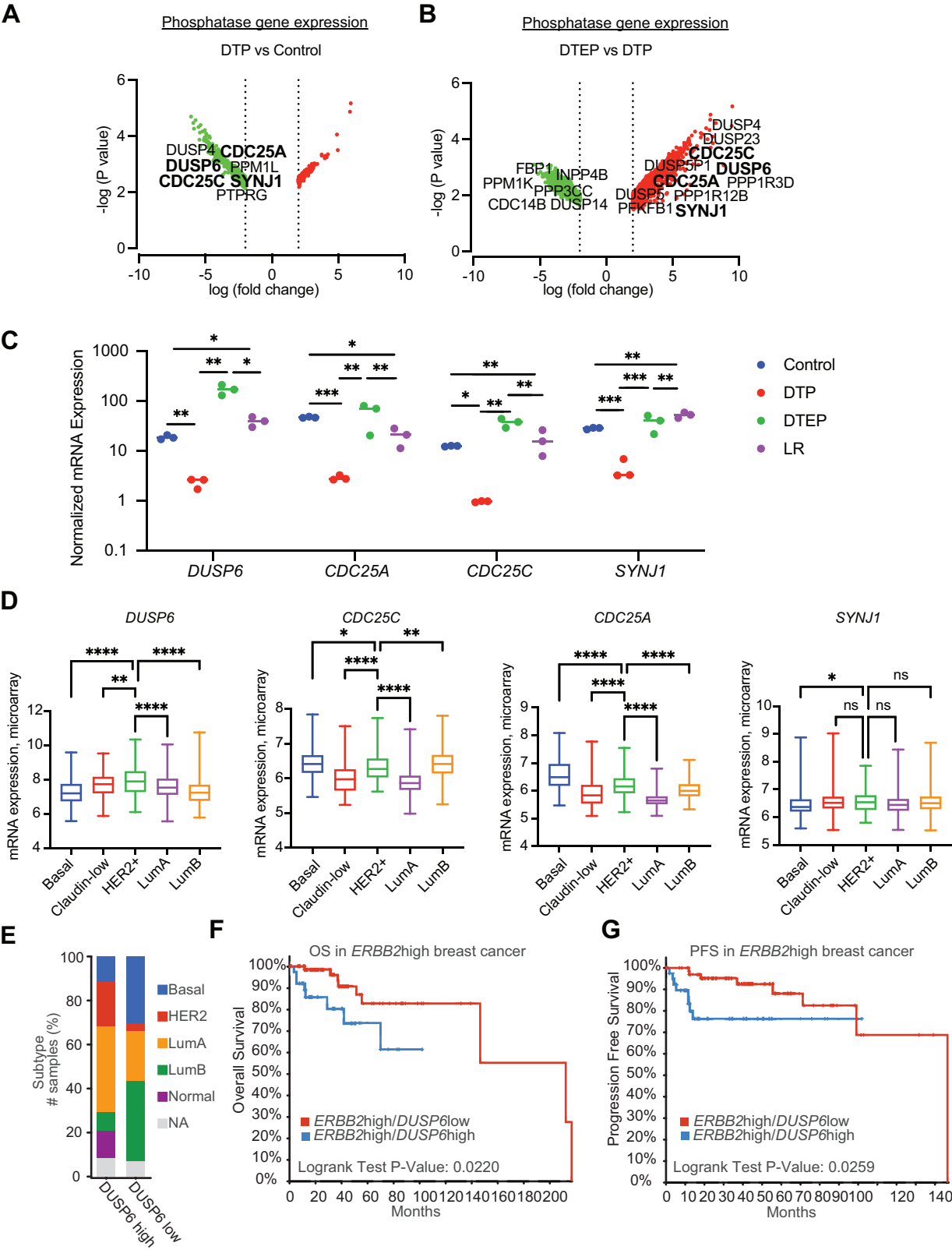
1542

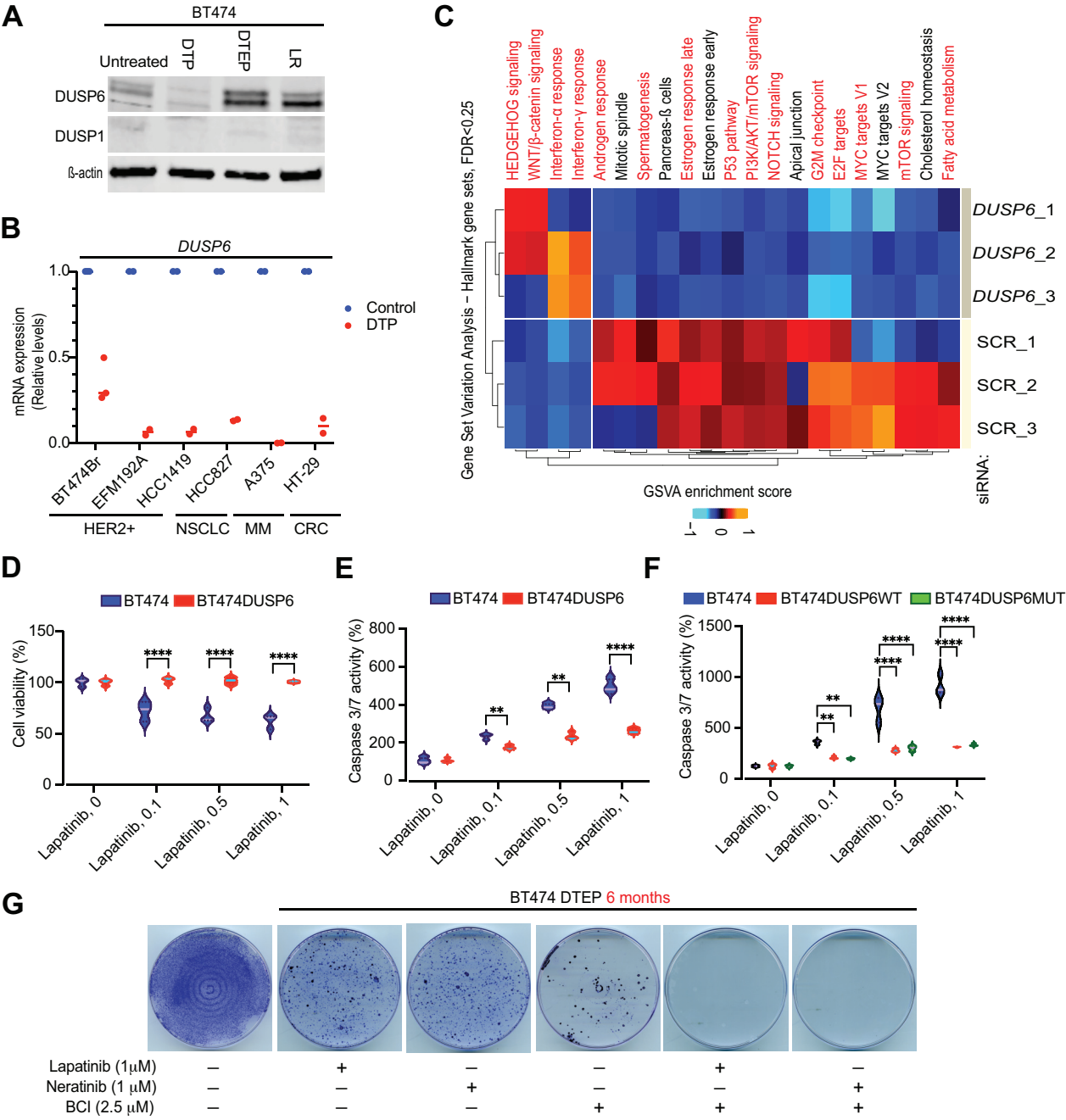
1543 **Figure EV4: The anti-proliferative activities of a library of small molecule**
1544 **modulators of phosphatases, kinases, and anti-apoptotic proteins in HER2i**
1545 **resistant cells.** The indicated cells were treated with the increasing concentrations
1546 (in μM) of the compounds for 48 h and cell viability was measured using WST-1
1547 assay. The long-term resistant (LR) BT474 and BT474Br generated *de novo* by 9-
1548 month treatment with lapatinib in this study had comparable drug sensitivity profile to
1549 acquired resistant cell line MDA-MB-453. The primary target of the used compound
1550 is indicated in parenthesis.

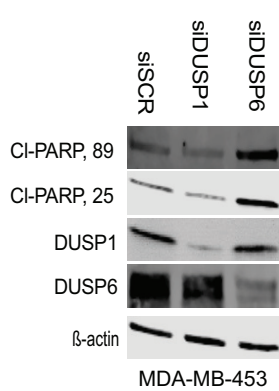
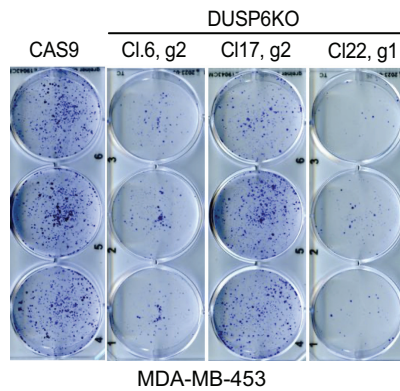
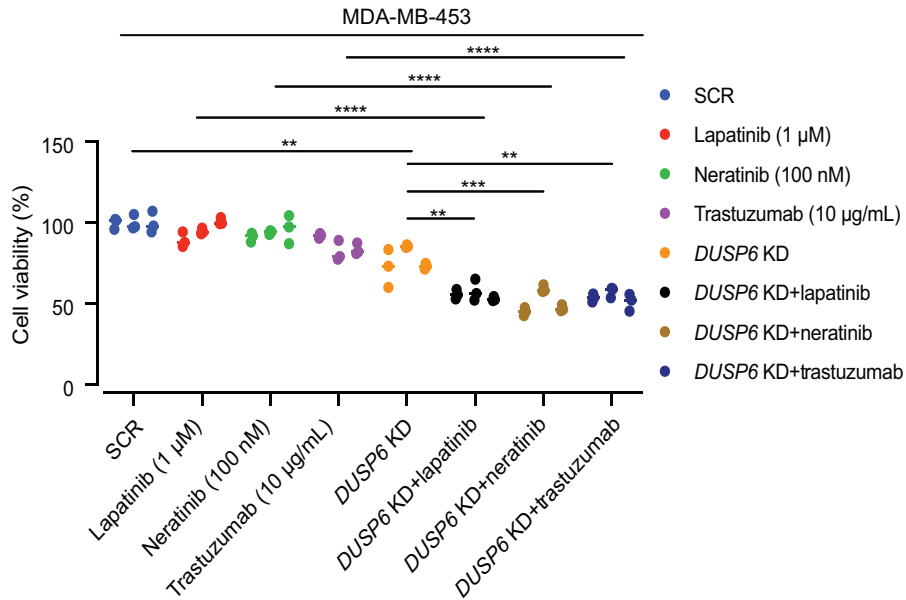
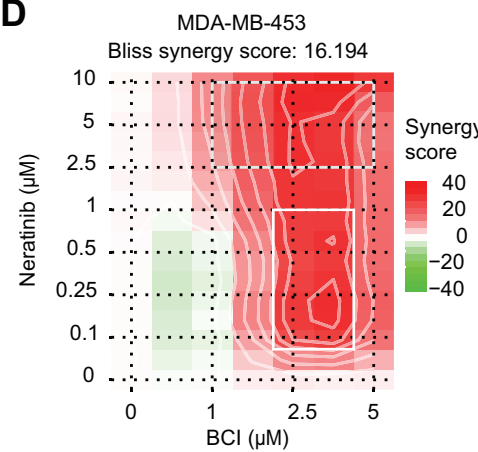
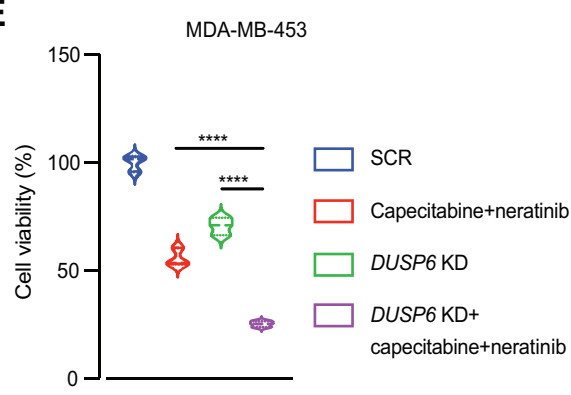
1551

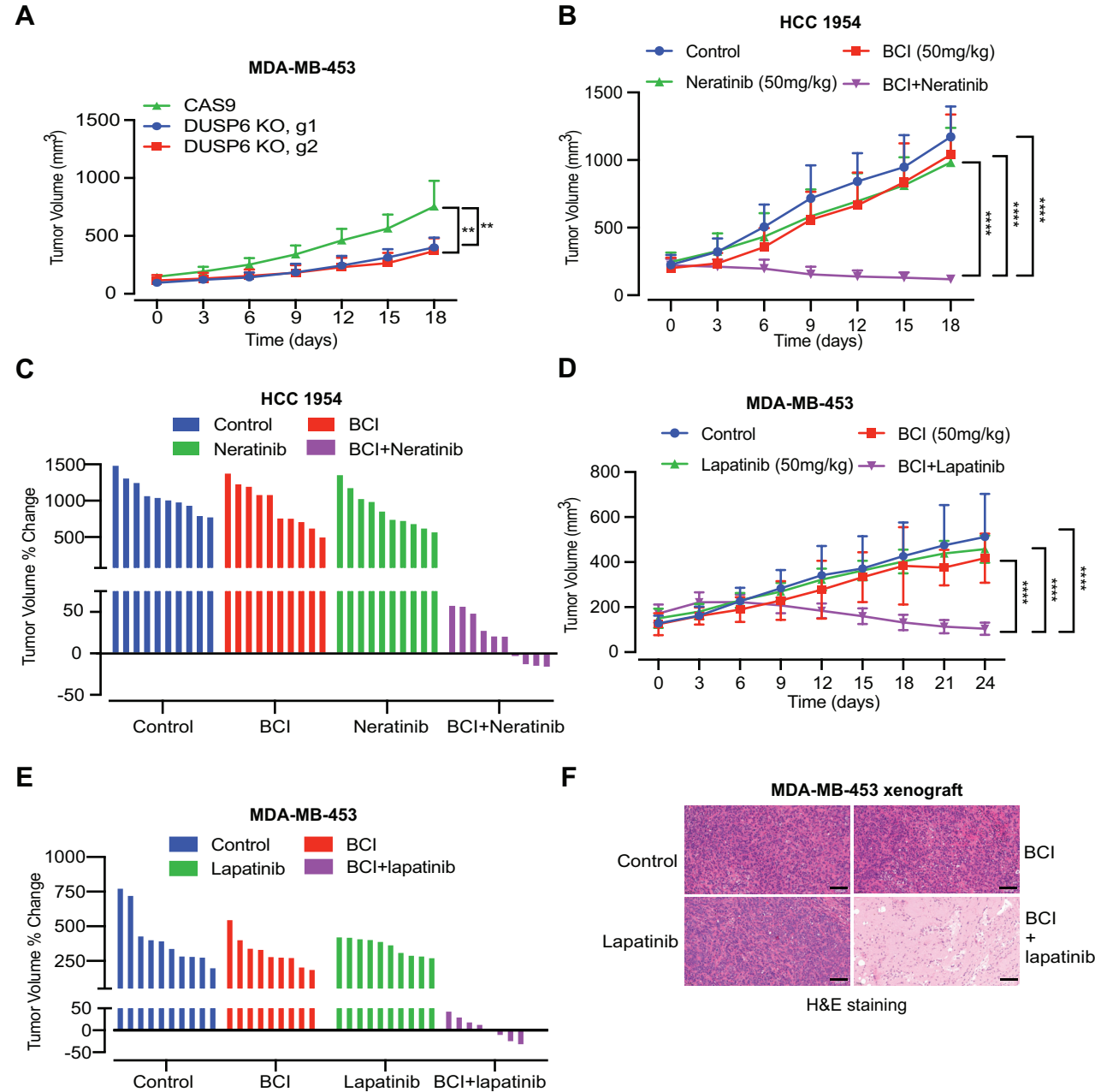
1552 **Figure EV5: Lack of DUSP6 inhibition is associated with HER2i resistance**
1553 **(A,B)** The effects of tucatinib on DUSP6 expression and the signaling pathway
1554 activities in (A) HER2i sensitive (green) BT474 cells or (B) HER2i resistant (red)
1555 MDA-MB-453 and BT474BrLR cells. The cells were treated with increasing
1556 concentrations of tucatinib for 48 h, followed by Western blot analysis. **(C)** DUSP6
1557 expression in MDA-MB-453 cells is resistant to multiple HER2is including antibody
1558 therapy with trastuzumab. The cells were treated with indicated drugs for 48 h,
1559 followed by Western blot analysis.

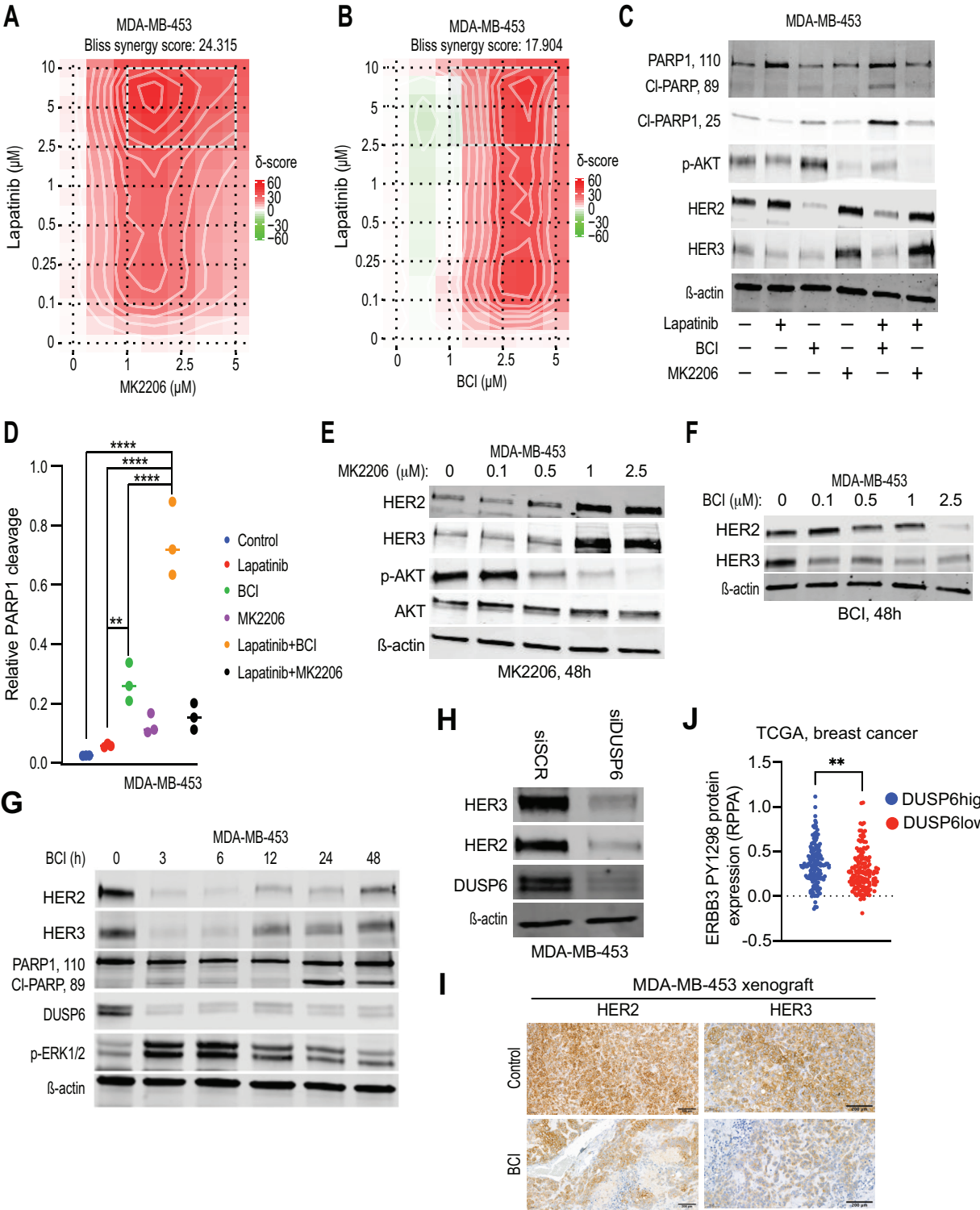
A**B****C**

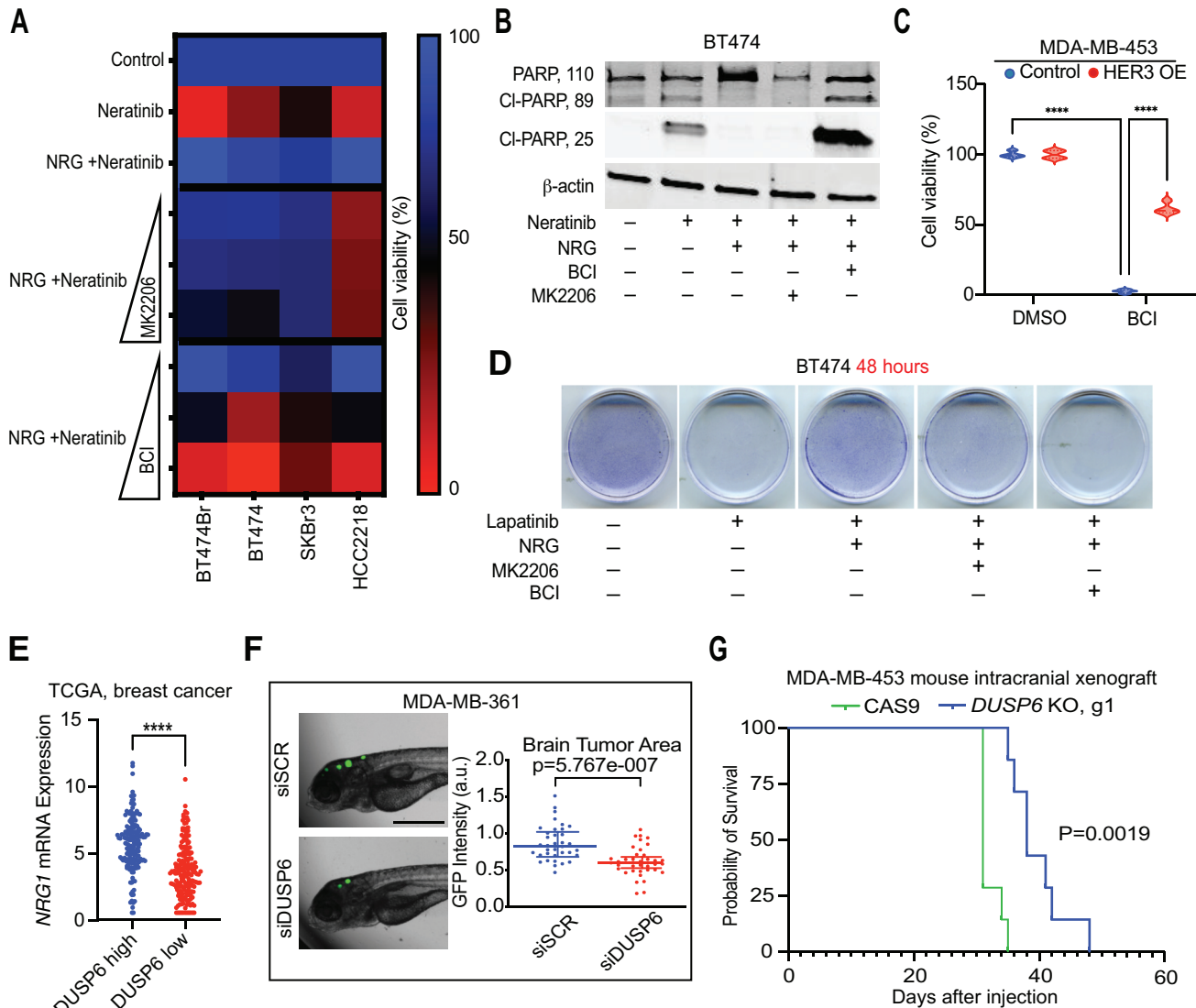


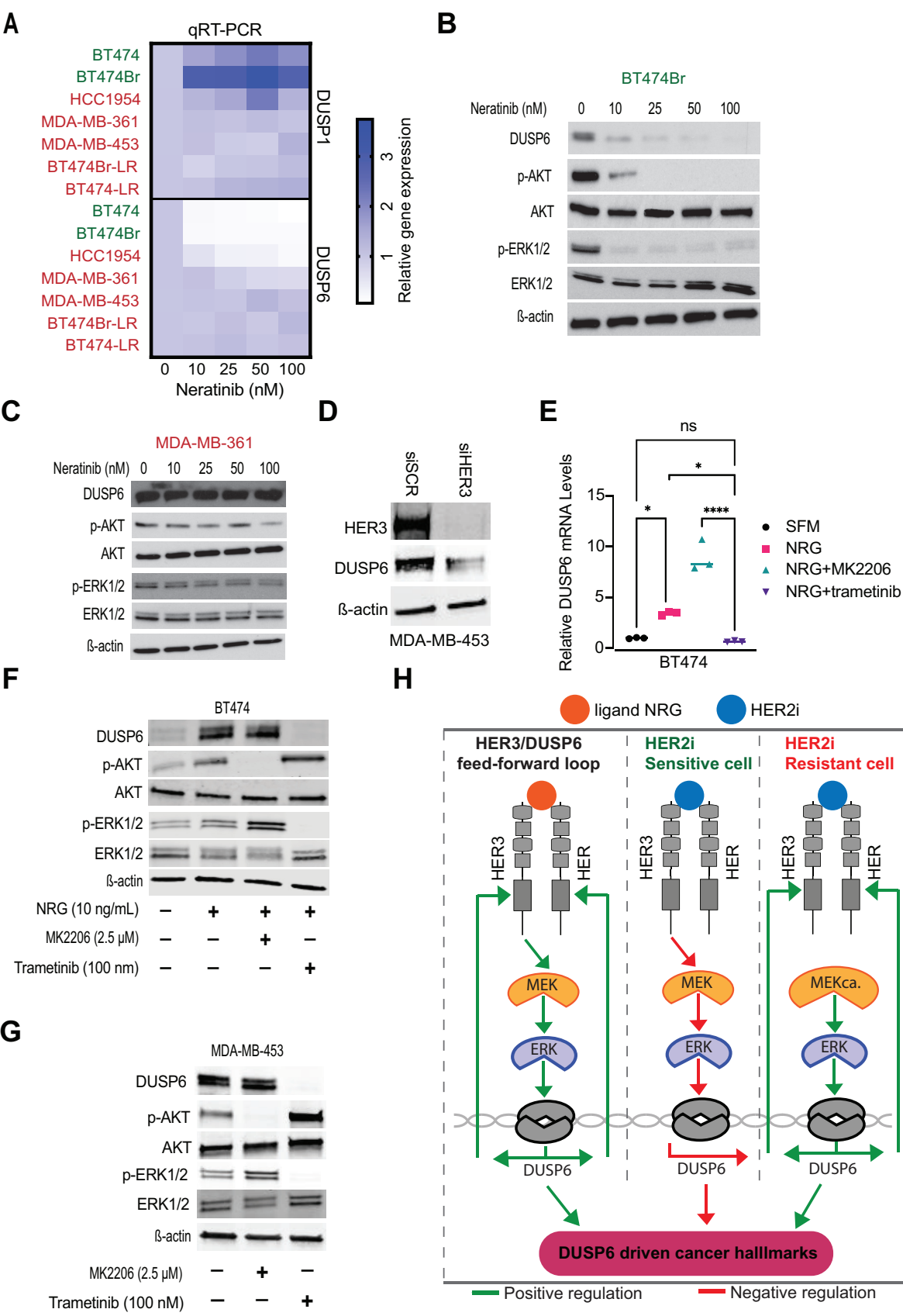


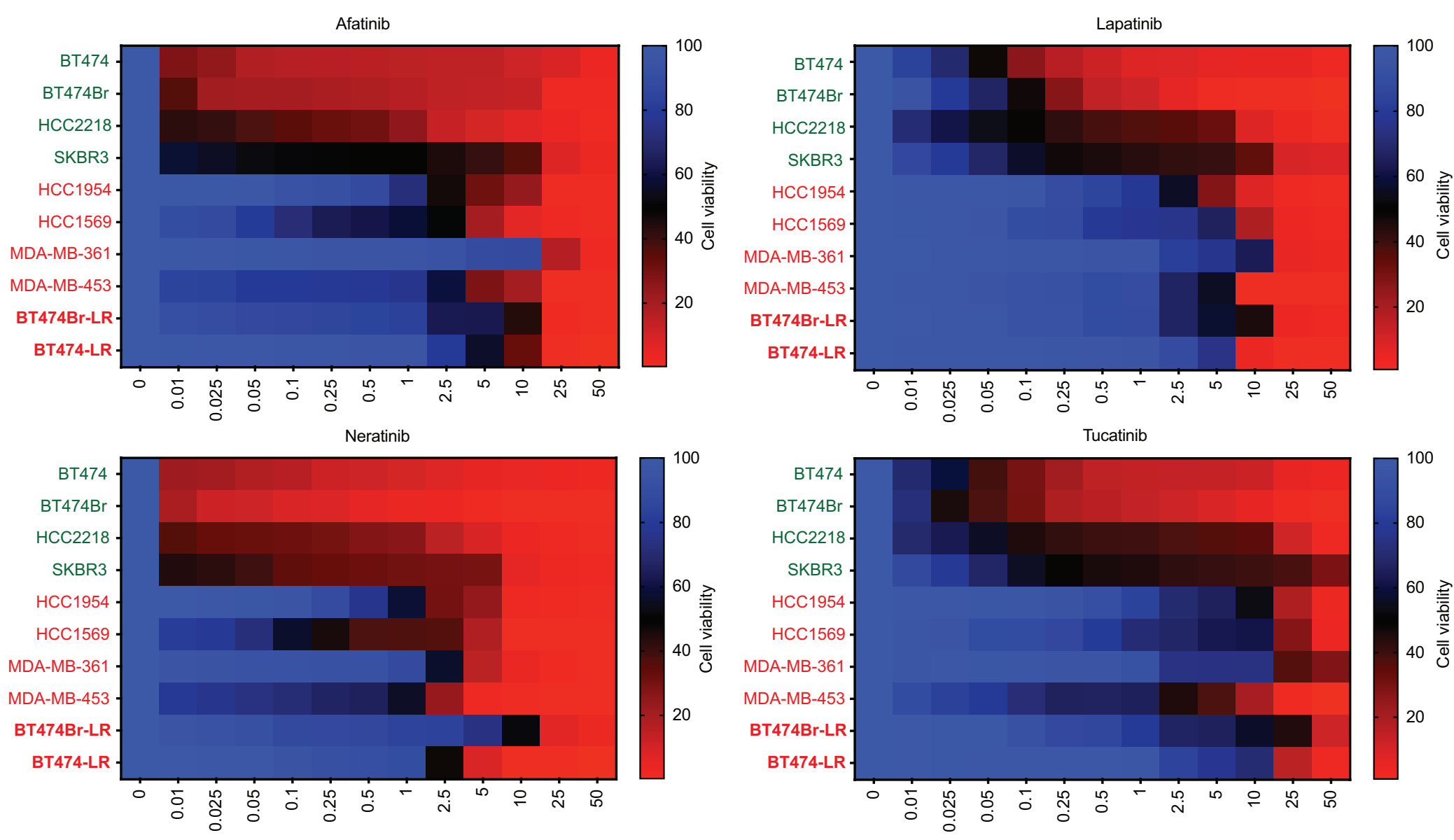
A**B****C****D****E**



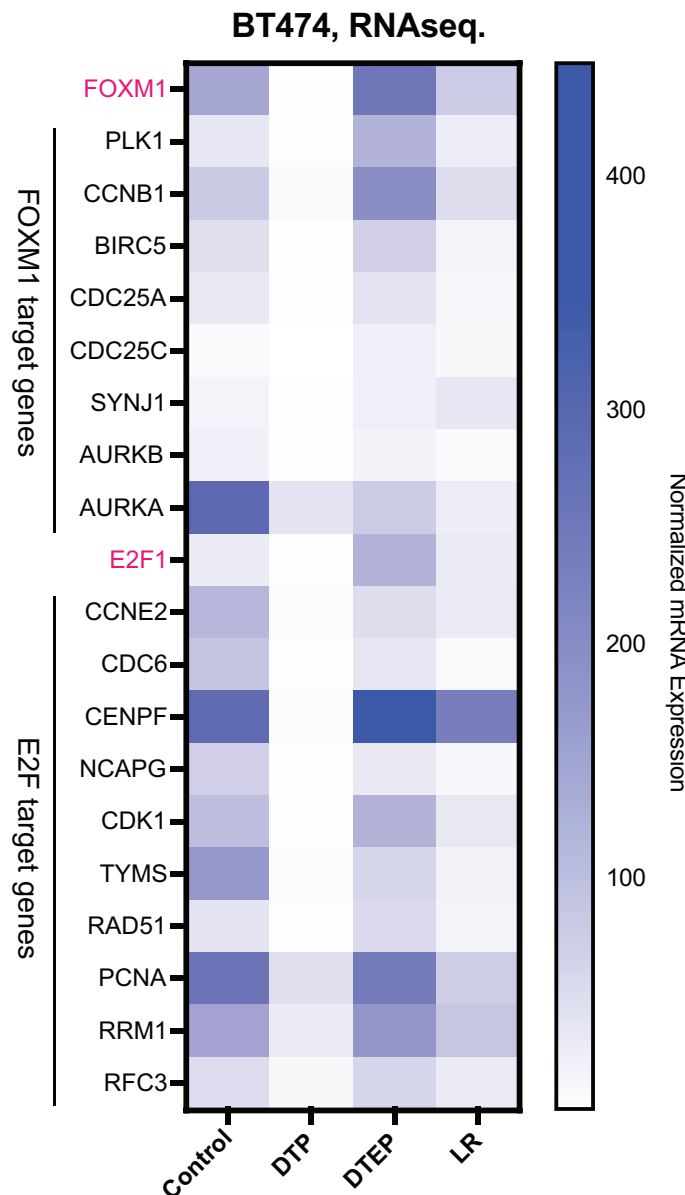




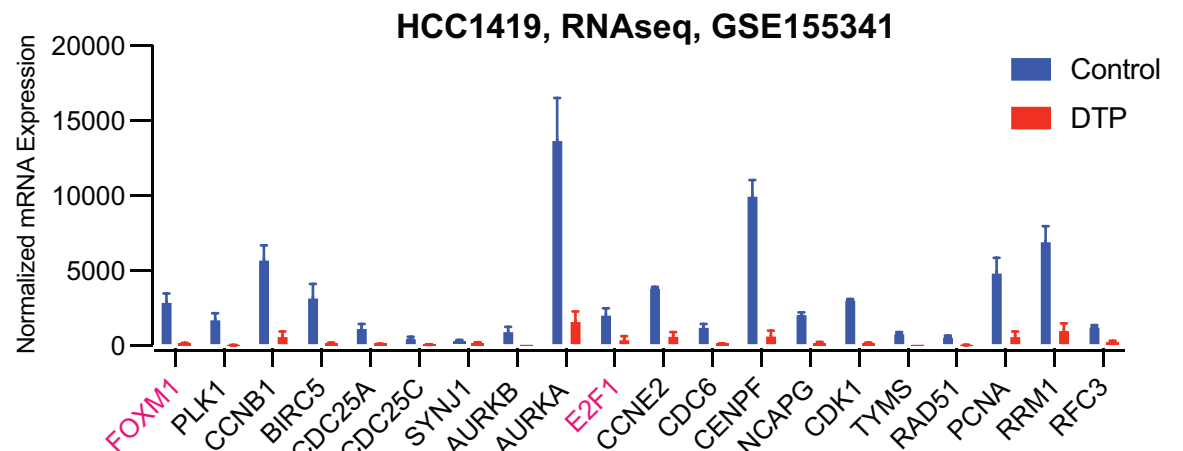
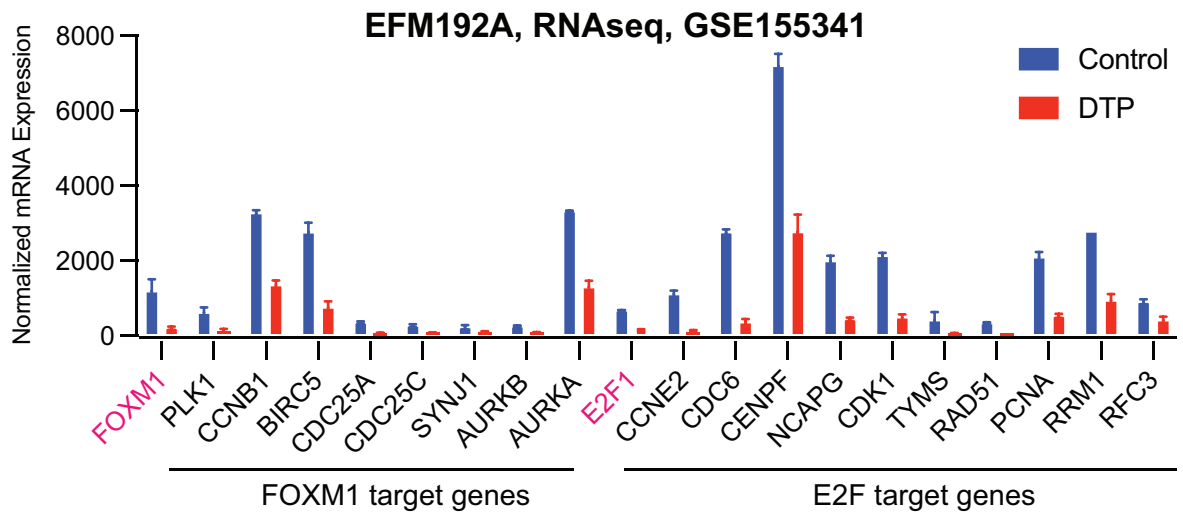
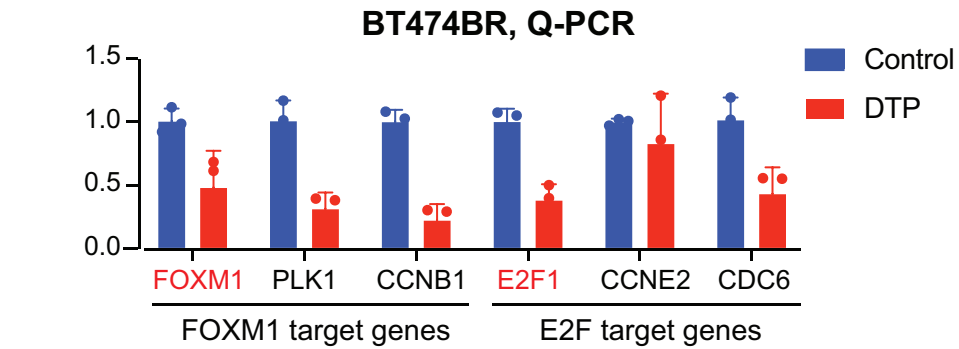


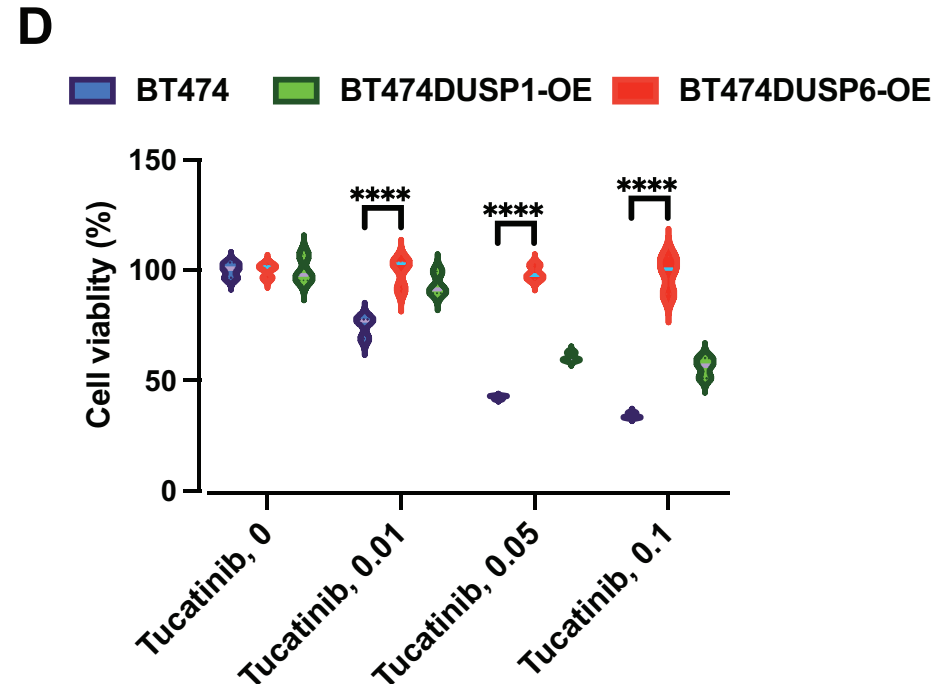
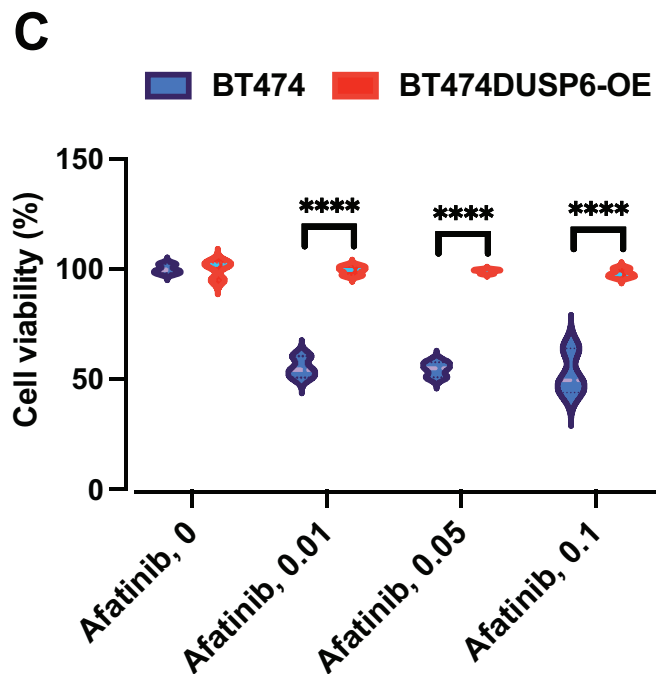
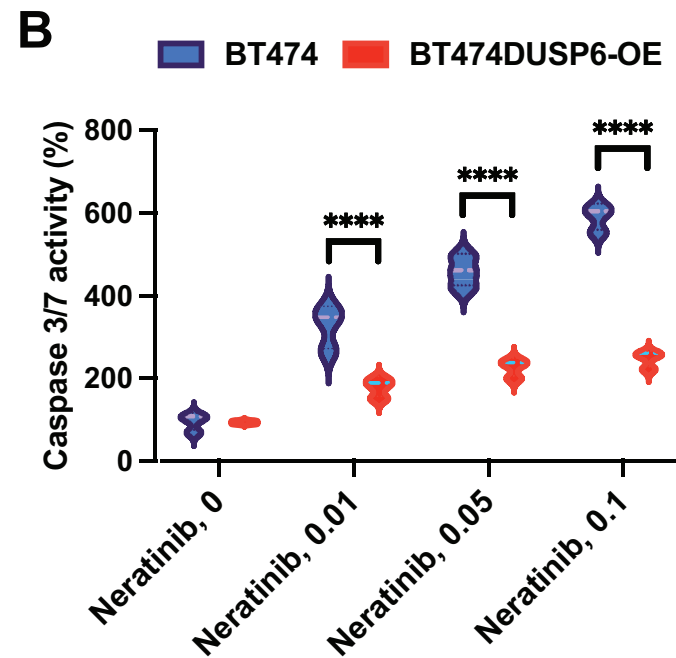
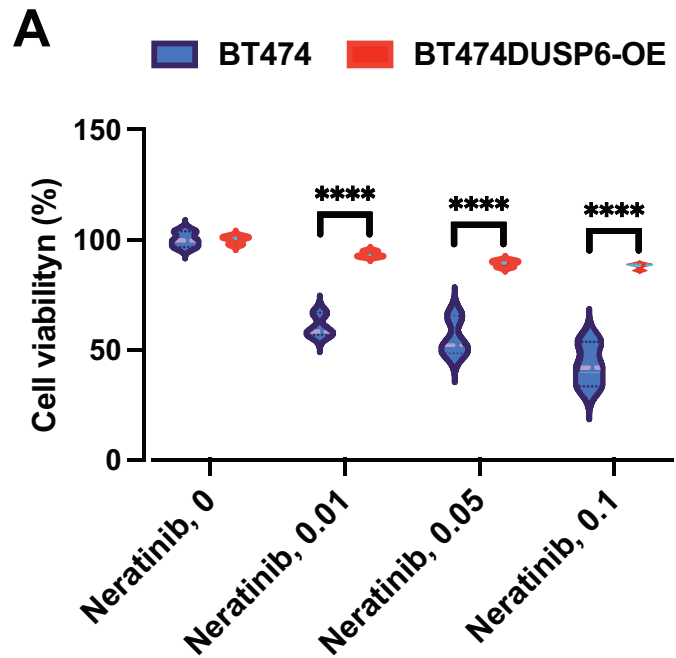


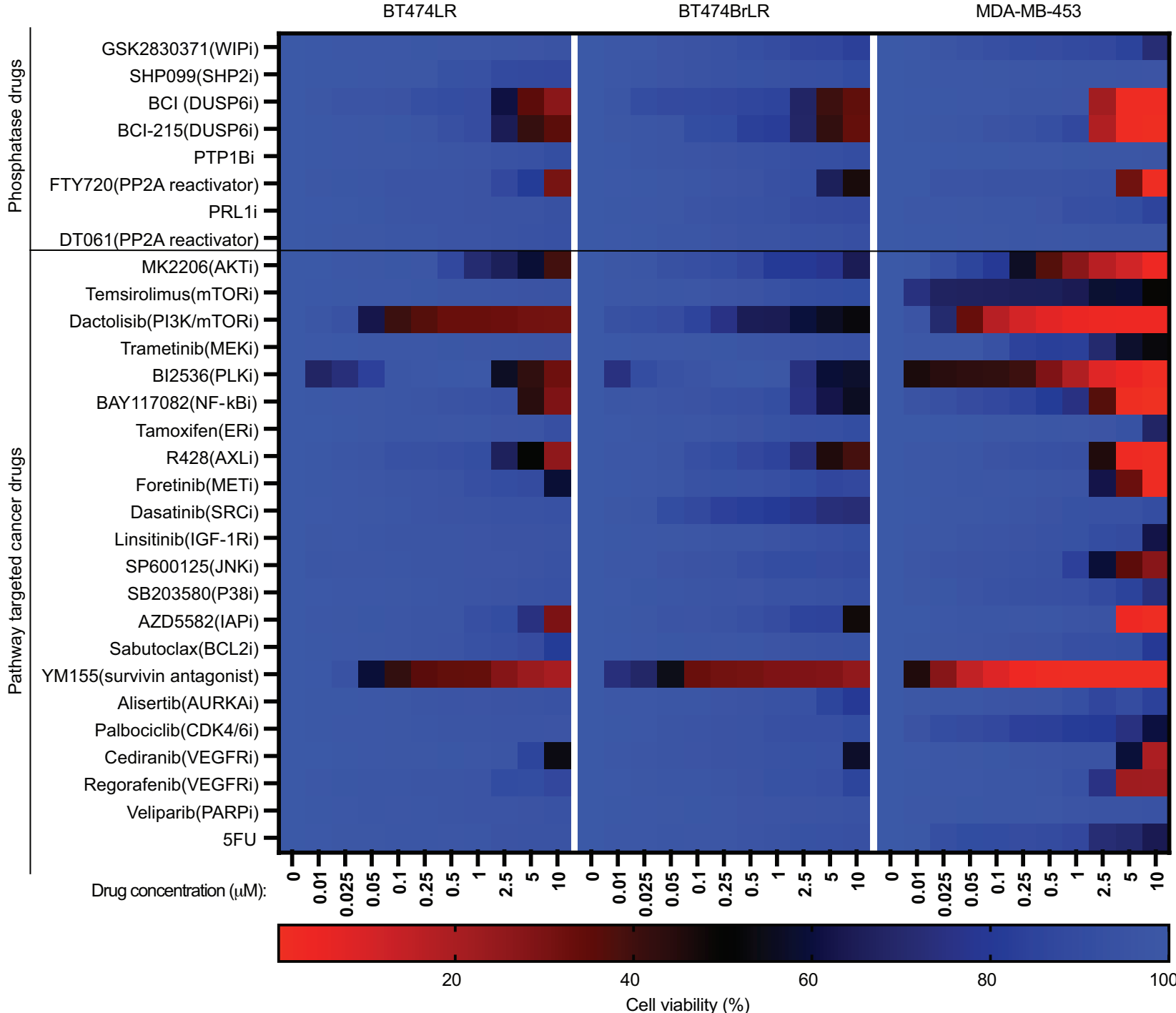
Expanded View 1

A

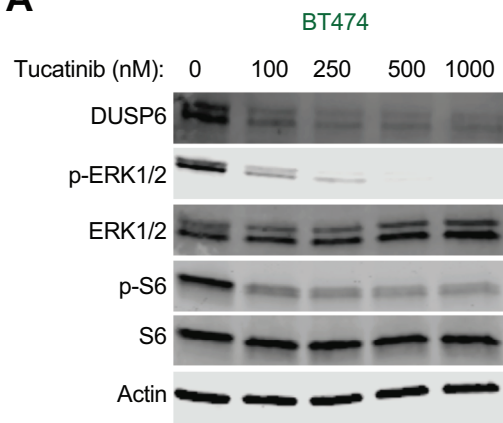
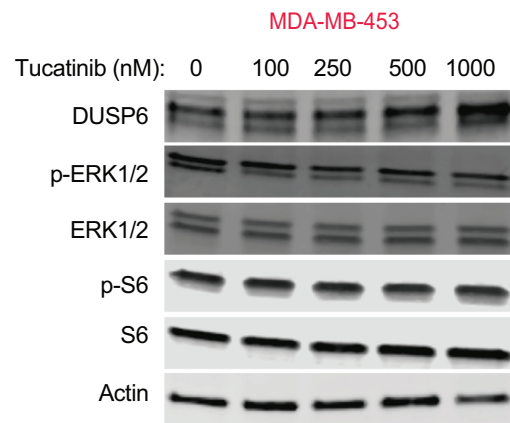
Expanded View 2

B**C****D**

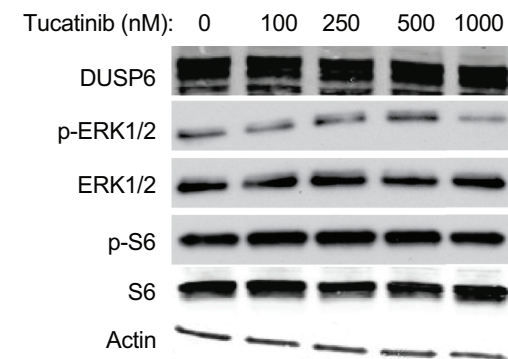
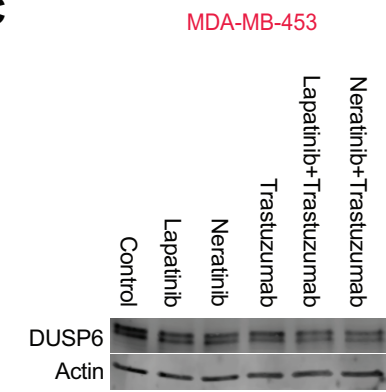




Expanded View 4

A**B**

BT474BrLR

**C****Expanded View 5**

Expanded view table 1:

Used siRNA sequences

Target Gene	Cat number	Company	Concentration
<i>HER2</i>	s613	ThermoFisher	20 nM
<i>HER3</i>	SI02660245	Qiagen	100 nM
<i>AKT1</i>	s659	ThermoFisher	20 nM
<i>DUSP1</i>	SI03100048	Qiagen	150 nM
	SI03106404	Qiagen	
	s4379	ThermoFisher	150 nM
<i>DUSP6</i>	s4378	ThermoFisher	
Negative controls	SI03650318	Qiagen	-
	4390844	ThermoFisher	
	4390847	ThermoFisher	

Expanded view Table 2:**Antibodies**

Target protein	Cat number	Company	Clone	Dilution
HER2	sc-33684	Santa Cruz	3B5	1:500-1:5000
p-HER2	2243	CST	6B12	1:1000
HER3	12708	CST	D22C5	1:1000
	05-390	Millipore	2F12	1:500
p-HER3	4791	CST	21D3	1:1000
DUSP1	07-535	Millipore	-	1:500
DUSP6	ab76310	Abcam	EPR129Y	1:1000
AKT	sc-5298	Santa Cruz	B-1	1:500
p-AKT	4060	CST	D9E	1:1000
ERK1/2	sc-514302	Santa Cruz	C-9	1:1000
p-ERK1/2	9101	CST	-	1:1000
β-actin	sc-47778	Santa Cruz	C4	1:5000
P38	8690	CST	D13E1	1:1000

p-P38	4511	CST	D3F9	1:1000
JNK1/2	3708	CST	2C6	1:1000
p-JNK1/2	4668	CST	81E11	1:1000
PARP-1	9532	CST	46D11	1:1000
CI-PARP-1	5625 ab32064	CST Abcam	D64E10 E51	1:1000 1:2500
GAPDH	5G4-6C5	HyTest	-	1:5000

CST: Cell signaling technology.

Expanded view Table 3

qRT-PCR primers

Gene	Accession number	Forward primer (5'→3')	Reverse primer (5'→3')	Size (bp)
<i>DUSP1</i>	NM_004417	AGGCCATTGACTTCATAGACTCC	TGGGAGAGATGATGCTTCGC	177
<i>DUSP6</i>	NM_001946	CCTGGAAGGTGGCTTCAGTAA	GCACTATTGGGGTCTCGGTC	180
<i>B2M</i>	NM_004048	GATGAGTATGCCTGCCGTGT	CTGCTTACATGTCTCGATCCC	79
<i>HER3</i>	NM_001982	GGTGATGGGAACCTTGAGAT	CTGTCACTTCTCGAATCCACTG	80
<i>HER2</i>	NM_004448	TGTGACTGCCTGTCCCTACAA	CCAGACCATAAGCACACTCGG	152
<i>BIRC5</i>	NM_001168	CCAGATGACGACCCCATAGAG	TTGTTGGTTTCCTTGCAATT	152
<i>E2F1</i>	NM_005225	TGGACTCTTCGGAGAACTTCA	TGATCCCACCTACGGTCTCC	93
<i>CCNE2</i>	NM_057749	TAGCTGGTCTGGCGAGGTT	GGCCTGGATTATCTGGGCTT	130
<i>CDC6</i>	NM_001254	GCGAGGCCTGAGCTGTG	AGGCAGGGCTTTACACGAG	181
<i>CENPF</i>	NM_016343	CGTCCCCGAGAGCAAGTTA	GTAAGGCAGCCCTTCTTCCA	98
<i>NCAPG</i>	NM_022346	AGTCCACATAGAGAAGAATGATGC	TCCACAGCATCCCAAGCATA	199
<i>CDK1</i>	NM_001786	AAACTACAGGTCAAGTGGTAGCC	TCCTGCATAAGCACATCCTGA	148
<i>TYMS</i>	NM_001071	CTGCTGACAACCAAACGTGTG	GCATCCCAGATTTCACTCCCTT	116

<i>RAD51</i>	NM_133487	CAACCCATTCACGGTTAGAGC	TTCTTGCGCATAGGCAACA	107
<i>PCNA</i>	NM_002592	GCGTGAACCTCACCAAGTATGT	TCTTCGGCCCTTAGTGTAAATGAT	76
<i>RRM1</i>	NM_001033	GCCAGGATCGCTGTCTCTAAC	GAGAGTGTGTTGCCATTATGTGGA	106
<i>RFC3</i>	NM_002915	GTGGACAAGTATCGGCCCTG	TGATGGTCCGTACACTAACAGAT	120
<i>ESCO2</i>	NM_001017420	TGTGTGCAAGTCTTGTGGTATG	CCCATCCCAAAACTCTGCTACT	145
<i>FOXM1</i>	NM_202002	ATAGCAAGCGAGTCCGCATT	AGCAGCACTGATAAACAAAGAAAAGA	151
<i>CDC25A</i>	NM_001789	CTACCTCAGAAGCTGTTGGGA	AAAGGCTTCATTTCCCTGTTCTCA	117
<i>AURKB</i>	NM_001313950	ACCTGCACCACATCCAACATC	TGCCAACTCCTCCATGATCG	164
<i>PLK1</i>	NM_005030	TCTTCCAGGATCACACCAAGC	AGGAGACTCAGGCGGTATGT	100
<i>CCNB1</i>	NM_031966	GATACTGCCTCTCCAAGCCC	TGACTGCTTGCTCTTCCTCAA	196
<i>CDC25C</i>	NM_001287582	CTACCCAGTCGGAAGGCAGA	AAACAAAACCTAGCTCAAGCCT	159
<i>AURKA</i>	NM_001323303	CTCAGTGGCGGACGAGGA	GGAGTGAGACCCTCTAGCTGT	200
<i>SYNJ1</i>	NM_003895	AGCTCTGAAGGGAAAGCGAA	TGTCTGCTCAGAACACGCAA	193